# The importance of microbiota and terrestrial inflows in controlling seston C:N:P:O:Si:Ca:Mn:Mg:Fe:K:Na:Cl:S:Cu:Zn stoichiometry of a deep coastal fjord

**Svein Rune Erga · Mikal Heldal · Siv Prestegard ·**
**Svein Norland · Tatiana Tsagaraki ·**
**Julia E. Storesund** [ORCID]

**Abstract** Comprehensive fjord-systems represent major extensions of the coastline and are therefore important transfer zones of materials from land to ocean. Despite increased terrestrial inflows to fjords due to climate changes, we know little about the effects on the ecosystem, especially biogeochemical cycling. We present novel data on spatiotemporal variations of seston multielement stoichiometry in the Sognefjord, the second longest (204 km) and deepest (1308 m) fjord in the world, relative to environmental conditions and microbiota. Concentration of major elements was highest in the upper brackish layer whereas trace metals and minor elements were highest close to the bottom. Seasonally varying microbiota was an important part of the seston in surface waters. None of the seston C:N:P (molar) annual means at specific depths corresponded to the Redfield ratio (106:16:1). At 5 m, annual means of N/P and C/N were 8.4 and 6.5, respectively, while at depth (50–1220 m) N/P were on scale 3 times higher (21–31) and C/N 3 times lower (1.6–2.6), suggesting alternative N-sequestration mechanisms. Overall, correlations between C-Ca and C-S indicate a strong influence from calcite ($CaCO_3$) and organosulfur producing microorganisms, while correlations between particulate Si and Mg–K–Ca–O at depth are consistent with clay and sinking diatom frustules. Mn concentrations increased strongly towards the bottom, likely from resuspension of $MnO_2$ rich sediments and clay particles. Based on seston concentrations, we arrived at the following stoichiometric relationship: $C_{55}N_{16}P_1Si_{3.6}Ca_{3.4}O_{16}Fe_{0.74}Mn_{0.51}Zn_{0.33}S_{0.21}Cu_{0.08}Cl_{1.7}Na_{0.68}Mg_{0.71}K_{0.37}$, although rarely measured, such information is a prerequisite for evaluating environmental impact on coastal ecosystems, biogeochemical cycling, pollution risk analysis and monitoring guidelines.

**Keywords** Seston · Coast-fjord · Elemental stoichiometry · Terrestrial runoff · Spatio-temporal variations · Advection

S. R. Erga · M. Heldal · S. Prestegard · S. Norland ·
T. Tsagaraki
Department of Biological Sciences, University of Bergen, Bergen, Norway

J. E. Storesund (✉)
Section of Contaminants and Biohazards, Institute of Marine Research, Bergen, Norway
e-mail: Julia.Storesund@hi.no

## Introduction

Marine coastal ecosystems worldwide are exposed to increasing inflows of chemical compounds from air-, land-, freshwater- and marine-sources (Crain et al.

2009). Fjords are important parts of the land–ocean continuum, and act as transition zones between terrestrial ecosystems and the open ocean. Due to enhanced environmental threats, they have been categorized as "Aquatic Critical Zones", with a need for increased attention (Bianchi et al. 2020). The Norwegian coastal landscape is dominated by fjords, seven of them being more than 100 km long, resulting in a coastline of approximately 21,000 km (Erga et al. 2012). Because of their size, several of the fjord systems are recognized as miniature oceans, but they are also an integral part of the coastal circulation dynamics. Fjords are classified as productive with respect to plankton biomass due to regular nutrient supplies by upwelling, (Aksnes et al. 1989; Aure et al. 1996, 2007; Asplin et al. 1999; Erga et al. 2012). This also makes them important nursery grounds for several commercial fish stocks (Berg and Albert 2003; Seitz et al. 2014; Skagseth et al. 2015). The microbial loop, functioning as the "backbone" of the marine food chain, comprises archaea, heterotrophic and photosynthetic bacteria, phytoplankton, nano-flagellates, and ciliates, is decisive for handling environmental emissions. Together, these microorganisms are responsible for assimilatory and dissimilatory processes, including primary production, mineralization of inorganic and organic matter, and bioremediation (Liermann et al. 2007; Pomeroy et al. 2007; Burgin et al. 2011). Light, salinity, temperature, oxygen, freshwater/terrestrial inflows, advection, competition for nutrients, grazing and viral lysis are crucial factors that structure microbial communities in coastal fjord environments (Storesund et al. 2015). Marine microbes are therefore considered living sensors of environmental threats such as climate change and pollution (Coelho et al. 2013; Gutiérrez et al. 2018).

Both freshwater- and saltwater-inputs have major impacts on fjords. In Norway, The Norwegian Coastal Current (NCC) is essential for the coupling between coastal- and fjord waters, flowing northwards along the coast and bringing with it water originating from the Baltic and southern North Sea (Sætre et al. 2007). Threshold fjords in Norway consist of a brackish upper layer (salinity < 33), identical with "Fjord water", above an intermediate layer of mixed brackish and NCC water (salinity between 33 and 34.99), and below sill depth the fjord basin that mainly originates from Atlantic water (AW) (salinity ≥ 35) (Svendsen 1981; Erga and Heimdal 1984; Sætre et al. 2007).

Freshwater together with tidal and/or wind generated advection (i.e., estuarine circulation) is crucial for the coastal-fjord water exchanges and give rise to both mixed and stratified water masses (Aure et al. 1996, 2007; Asplin et al. 1999; Erga et al. 2012). Vertical displacements within the lower pycnocline are controlled and maintained by internal waves (Inall and Gillibrand 2010; Støylen and Fer 2014). In addition, advection (e.g., upwelling) is important for pelagic-benthic fluxes of particulate and dissolved matter (including nutrients), regulation of productivity, and for resuspension of sediments (crustal enrichment) (Wassmann 1984; Stabholz et al. 2013).

Runoffs from hydroelectric power plants are regulated and occur highly concentrated at specific sites. They are therefore among the most highlighted environmental stressors of many fjord systems (Myksvoll et al. 2014). Natural freshwater runoffs discharge large quantities of dissolved and particulate matter to the fjord, originating from lithogenic, soil, limnic, and anthropogenic sources. Suspended particulate matter (SPM)/seston consists of both organic and inorganic material, dominated by particles less than a few hundred microns in diameter (Reynolds et al. 2010; Ehn et al. 2019). In coastal-fjord waters inorganic particles originates from erosion of rocks, amongst which clay (< 2 μm) and silt (2–63 μm) particles are most important (Aarseth et al. 1989; Klitgaard-Kristensen and Buhl-Mortensen 1999; Paetzel and Dale 2010). Glaciomarine sediments are dominant in western Norwegian fjords and can be more than 300 m in thickness (Aarseth et al. 1989), with some contributions from marine silicate and carbonate production (Paetzel and Dale 2010; Faust et al. 2017). It is expected that increased precipitation, weathering, and ice melting associated with future climate changes will lead to enlarged inputs of terrigenous materials to the fjords (Faust et al. 2014).

The literature on SPM elemental stoichiometry often focusses on the classic Redfield C:N:P atomic ratio: 106:16:1 (Redfield et al. 1963; They et al. 2017), even though a number of studies reveal large discrepancies from the Redfield ratio, particularly in large datasets (Schneider et al. 2003; Arrigo 2005; Martiny et al. 2014; Sharoni and Halevy 2020). In a greater perspective the concept of ecological stoichiometry should preferentially be used to describe the balance of chemical elements in ecological interactions (Sterner and Elser 2002), and information on

essential elements beyond C-N-P are prerequisite to better ascertain which particles are involved and their origin. C, N, H and O are major elements of all organic molecules, as well as the main constituents of proteins together with S. S is also involved in photosynthesis, while P is important for energy storage (e.g., ATP) and in nucleic acids (Taiz and Zeiger 2006; Merchant and Helmann 2012). In addition, Ca is an important structural compound in coccolithophorids and foraminifers ($CaCO_3$ cell cover), whereas Si has the same function in diatoms, silico-flagellates, and radiolarians (cell wall of $SiO_2$). Further, many essential elements such as K, Mg, Mn, Fe, Zn, Cu, Ni and Mo are cofactors in enzymes, or constituents in cytochromes (Fe) and chlorophylls (Mg). Finally, Cl is required for photosynthesis (Raven 2017), and is together with Na, K and Ca involved in osmotic regulation and signaling pathways in plant cells, marine bacteria, cyanobacteria, and archaea (Martin et al. 1999; Heldal et al. 2003, 2012; Taiz and Zeiger 2006; Helliwell et al. 2021). Chemical composition of clay particles usually comprises oxides of Si, Fe, Al, Ca, Mg, Mn, K and Na (Ndzana et al. 2019). It should be noted that the intracellular pool of dissolved elements in living cells are operationally particulate.

The main objective of this study was to investigate how seston C:N:P:O:Si:Ca:Mn:Mg:Fe:K:Na:Cl:S:Cu:Zn elemental concentration and stoichiometry of a deep coastal-fjord system is affected by environmental conditions during an annual cycle, with special emphasis on land-fjord and fjord-coast interactions, and the role of microbiota.

Our results show large vertical differences in elemental stoichiometry and may lead to a better understanding of how biogeochemical cycling operates within a highly dynamic and integrated land-fjord-coastal system. From a climate change and monitoring context, the wide range of elements investigated may serve as future reference with respect to environmental status.

## Materials and methods

### Description of the study site

The site of this investigation, the Sognefjord (SF) (Fig. 1), is 205 km long, has a mean width of 4.5 km, and a maximum depth of 1308 m, making it the second largest fjord in the world. In the inner part the SF splits into several side-fjords, most with shallow sills (< 20 m). At the mouth, the SF is separated from the coastal water by a sill at 170 m depth. The fjord system has a surface area of 1000 $km^2$ and a volume of 500 $km^3$, about 1% of the North Sea volume. The yearly freshwater inflow to the SF amounts to 8.2 $km^3$ $year^{-1}$ (Grøttå et al. 2016), representing > 1% of its total volume.

### Sampling and analysis

Sampling was conducted onboard "R/V Hans Brattstrøm" in the outer part of the fjord (Brekke, depth 1250 m, 61°02.42′ N, 5°25.01′ E), at selected depths using 2.5 L Niskin bottles, at nine time-points between 27 June 2012 and 31 July 2013. Temperature, salinity, density, dissolved oxygen, and chlorophyll *a* (chl *a*) fluorescence measurements were obtained with a CTD (Conductivity-Temperature-Depth), type SAIV-SD 204, with salinity, temperature, and chl *a* fluorescence accuracy of $\pm 0.02$ ppt, $\pm 0.01$ °C, and $\pm 0.03$ μg $L^{-1}$, respectively. The CTD temperature sensor was calibrated before use. Salinity was calibrated by measuring salinity of samples collected from the deepest sampling level on each cast using a Guildline 8400 AutoSal with IAPSO Standard Sea Water as a reference. Oxygen concentrations in mL $L^{-1} \pm 0.01$ were measured by titration using the Winkler method (Andersen and Føyn 1969) at selected dates and depths. Apparent Oxygen Utilization (AOU) (mL $L^{-1}$) was calculated as the difference between the measured dissolved oxygen concentration and its equilibrium saturation concentration in water with the same physical and chemical properties.

Samples for dissolved inorganic nutrients nitrate ($NO_3^-$), nitrite ($NO_2^-$), phosphate ($PO_4^{3-}$), and silicate ($Si(OH)_4$) were collected from standard depths: 0.5 m, 5 m, 10 m, 50 m, 100 m, 150 m, 200 m, 400 m, 800 m, 1000 m, 1200 m, and 1220 m. The samples (unfiltered) were immediately preserved with chloroform (200 μL per 50 mL sample) and stored dark at 4 °C until analysis. Chloroform blank levels were safely below analyzed nutrient levels. Nutrient analyses were performed at the Institute of Marine Research in Bergen, Norway using an autoanalyzer (Alpkem-Lab) according to Parsons et al. (1992). Ammonium ($NH_4^+$) concentrations were measured on fresh samples from standard depths
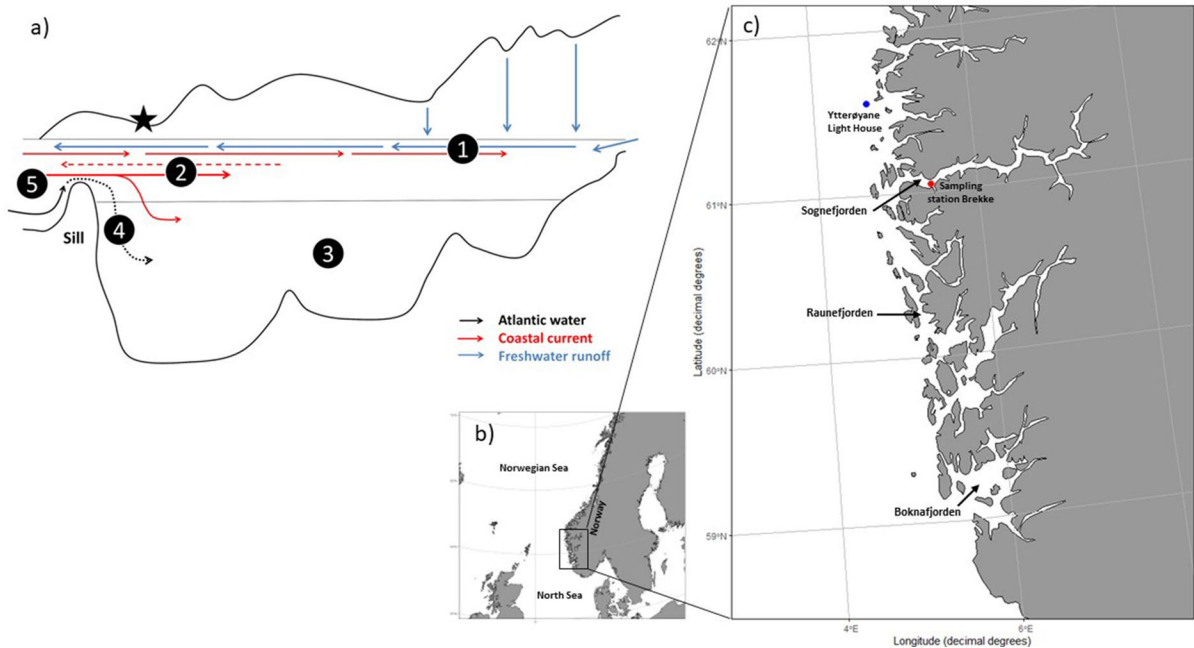
**Fig. 1** **a** Schematic illustration of the bathymetry of the Sognefjord (not to scale), indicating water masses and water mass origin. **1.** Surface water influenced by freshwater runoff (blue arrows) and coastal water in the counter current (red arrows). **2.** Intermediate water influenced mainly by coastal water. Stippled arrow indicates counter current transporting water out of the fjord. **3.** Basin water originating from Atlantic water (black arrows). Turbulence and mixing occur between all three water masses, gradually making the basin water less saline. Given high enough salinity and favoring wind-regimes outside the sill **(5.)** heavy Atlantic water may enter the fjord and replace the resident water **(4.)**. The approximate location of sampling station Brekke is marked with a star. **b** An overview map and **c** detailed map indicate the location of Sognefjorden, Raunefjorden and Boknafjorden on the west coast of Norway, where the red dot represents the location of Brekke in the Sognefjord and the blue dot Ytterøyane lighthouse

using a microplate fluorometric technique based on the method of Holmes et al. (1999) and Poulin and Pelletier (2007), and further adapted and tested by Siv Kristin Prestegard. Acid washed glass equipment was used in all preparations of standards, incubation tubes and sample bottles.

Water samples for counts of single-celled phytoplankton, prokaryotes (bacteria and archaea) and viral abundances by flow cytometric measurements (FCM) were collected from the same depths as dissolved inorganic nutrients. Samples were fixed with glutaraldehyde (25%, final concentration 0.5%) for 30 min at 4 °C, flash frozen in liquid nitrogen and stored at − 80 °C. Prior to analysis, samples were diluted 10 to 1000-fold in TE buffer (10:1, pH 8), and stained with SYBRGreen-I (Molecular probes) which stains double-stranded DNA. Samples were analysed for 1 min at flowrates of ~ 30-35μL min$^{-1}$ (prokaryotes and viruses) or ~ 55–60 μL min$^{-1}$

(phytoplankton), using only the results from dilutions with 100–1000 events s$^{-1}$ (Marie et al. 1999, 2001; Larsen et al. 2004).

Samples (250–1500 mL) for qualitative and quantitative analysis of the elemental composition of SPM were taken at 5 m, 50 m, 200 m, 800 m, and 1220 m. In addition, a sample was taken at the bottom of the halocline when this was not coinciding with standard depths 50 or 200 m. These were 60 m on 27 June 2012, 170 m on 12 October and 11 December 2012, and 250 m on 5 February 2013. Samples for SPM elemental analysis were filtered in triplicate onto 0.6 μm pore size Poretics polycarbonate (PC) filters (47 mm), and 0.6–0.8 μm nominal pore size Whatman GF/F glass fiber filters (47 mm). Filters were then rinsed with 5 mL of reverse osmosis water to avoid salt precipitations; air dried and stored in Millipore petri slides until analysis by using a wavelength dispersive X-ray fluorescence (WDXRF) spectroscopy technique

adapted for marine samples in a Bruker AXE S4 Pioneer WDXRF instrument (Paulino et al. 2013). Using filter-specific calibrations a minimum of three blank filters were analyzed for each new batch of filters and relevant element reference standards were checked regularly. For further information on calibration, detection limits, precision and accuracy see Paulino et al. (2013). Two different filter types were used in these analyses to compensate for analytical interference from the elemental composition of the filters themselves. Data on C and N content were collected from the GF/F filters, while data on O, Si, Ca, Mn, P, Mg, Fe, K, S, Cu, Na, Cl, and Zn content were collected from the PC filters. Particular P was also measured on GFF filters and cross calibration with PC filters showed consistent results ($r^2 = 0.9$).

For scanning electron microscopy, 500 mL sample water was filtered onto 0.6 μm pore size Poretics polycarbonate filters (25 mm). The filters were air dried and stored in plastic tubes until further preparation. Specimens were prepared by mounting the filters on Al-stubs and coating them with Au/Pd in a Polaron SC502 Sputter Coater for 30 s. The specimens were viewed in a Zeiss Supra 55VP or a JEOL SCM 6400 scanning electron microscope at 250–3500×magnification or higher if necessary.

### Wind, current and water runoff data

Wind measurements from Ytterøyane lighthouse, situated outside the SF (Fig. 1), were obtained from the Norwegian Meteorological Institute's climate data base "eKlima" (http://eklima.met.no). These wind data are representative for the open coastline with no topographic obstacles. Current speeds were obtained by the current model NorKyst800 (https://www.hi.no/hi/temasider/hav-og-kyst/modeller) (see Storesund et al. 2017; Asplin et al. 2020, for further details). Data on water runoffs to the inner SF were kindly given by the Hydrology Department at Norwegian Water Resources and Energy Directorate (NVE) (http://www.nve.no/).

### Statistical analyses

Statistical analyses were done in R (R core team 2021) unless otherwise stated. Standard error of the mean (SEM) of particulate elements was calculated by taking the standard deviation and dividing by the square root of the sample size, and it is given for all sampling points. Detailed linear regression and elemental correlation matrix analysis were performed in Excel.

Unconstrained ordination (Principal Coordinates Analyses (PCoA)) was used to visualize and examine patterns of the elemental composition at the different sampling-times and depths in the fjord. Briefly, a dissimilarity matrix of the measured elements was constructed on square-root transformed data using the daisy function with Euclidean distances in the cluster package (v2.1.1; Maechler et al. 2019). A PCoA was then constructed on the resulting dissimilarity matrix using the ape package (Paradise and Schliep 2019). The 'betadisper' function in the vegan package (v2.5–7; Oksanen et al. 2020) followed by an anova was used to further examine potential differences in elemental composition between water layers by examining the dispersion of variances. To investigate the link between environmental variables and microorganisms on the elemental composition, a distance-based redundancy analysis (db-RDA) was constructed by running a redundancy analysis (RDA) on the primary and secondary axes obtained from the PCoA using the rda function in the vegan package. Temperature, salinity, density, $O_2$, chl *a* fluorescence, inorganic nutrients ($NO_3^-$, $NO_2^-$, $NH_4^+$, $Si(OH)_4$, $PO_4^{3-}$) and microbial counts (Prokaryotes, Nanophytoplankton, Picophytoplankton, *Synechococcus*) were used as constraints. To look at the individual effects of dissolved inorganic nutrients and the microbial community respectively, one db-RDA was constructed using only oxygen and inorganic nutrient concentrations as constraints, and one using only microbial counts and chl *a* fluorescence as constraints. To examine which individual variables that were most likely influencing the elemental community composition, an anova (999 permutations) was run on the three individual db-RDAs.

## Results

### Hydrography

Salinity and temperature varied between 14.47–35.27 and 3.67–16.99 °C (Fig. 2), with means of 34.93 and 7.62, respectively. The highest surface salinities were found during winter, while large freshwater
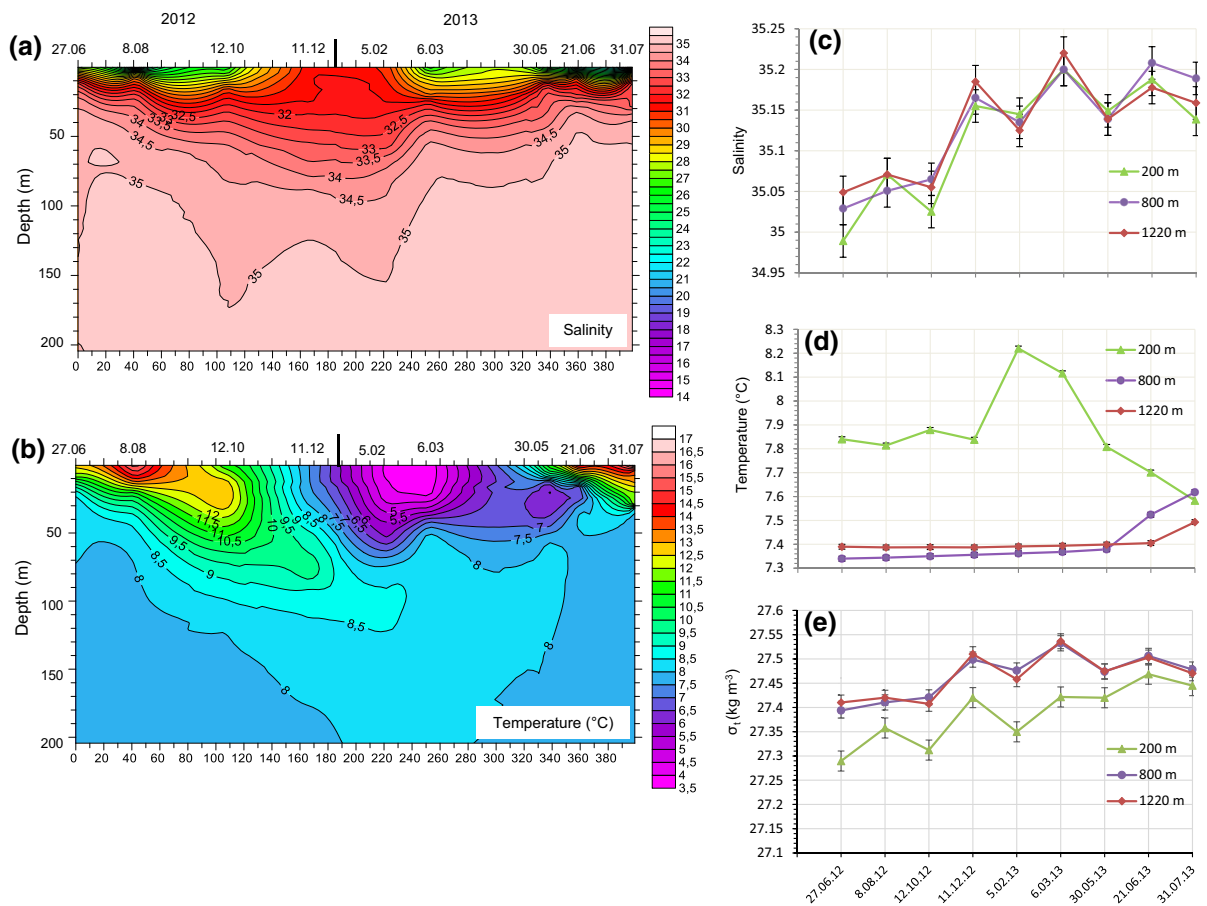
**Fig. 2** Salinity (S) and temperature (T, °C) in the Sognefjord from 27 June 2012 to 31 July 2013. Isopleth diagrams 0–200 m for **a** S and **b** T, and temporal variations at 200, 800 and 1220 m for **c** S, **d** T, and **e** density (σ_t, kg m$^{-3}$)

discharges in May–July, with daily means reaching 786 m$^3$ s$^{-1}$ in July 2012 (monthly mean 454 m$^3$ s$^{-1}$) and 754 m$^3$ s$^{-1}$ in June 2013 (monthly mean 376 m$^3$ s$^{-1}$) (Fig. 3), led to a more brackish surface layer during summer (Figs. 2a, S1a). Following periods with Northerly winds (Fig. S2) water with salinity of 33.00 was seen at 15–20 m in June-July. AW with salinity ranging from 35.00 to 35.22 and temperature from 7.34 to 8.20 °C was found shallower than 50 and 80 m in June 2013 and 2012, respectively. Below sill depth (170 m), variations in salinity and temperature were small, with AW dominating and temperatures ≥ 7.34 °C at all depths (Fig. S1a,b). In the basin layer, at 1220 m depth, salinities increased from 35.05 to 35.19 during the period October–December 2012, while the temperature remained the same (7.39 °C) (Fig. 2c, d). This led to an increase in

density (sigma-t) from 27.41 to 27.51 (kg m$^{-3}$) (Fig. 2e), which indicates an inflow and descent of dense AW across the sill in late autumn 2012. This was concomitant with prevailing strong Easterly-South Easterly coastal winds (Fig. S2). Salinities in the basin water remained at an elevated level from December 2012 until the end of the investigation period (31 July 2013), with minor variations between dates. In June-July 2013 the entire basin layer was relatively homogenous with respect to salinity and temperature, 35.13–35.19 and 7.49–7.62 °C, respectively, measured in July (Fig. 2c, d).

Oxygen conditions were non-stagnant, confirmed by saturation values varying from 112.05% in July 2013 at 5 m to 68.2% in February at 1220 m (Table S1). Below sill depth (170 m) oxygen saturation had a maximum of 88.9% in July at 800 m.

**Fig. 3** **a** Daily and **b** monthly means ($m^3\ s^{-1}$) in freshwater runoffs to the inner Sognefjord from May 2012–July 2013. Data were kindly given by the Hydrology Department at Norwegian Water Resources and Energy Directorate (NVE)
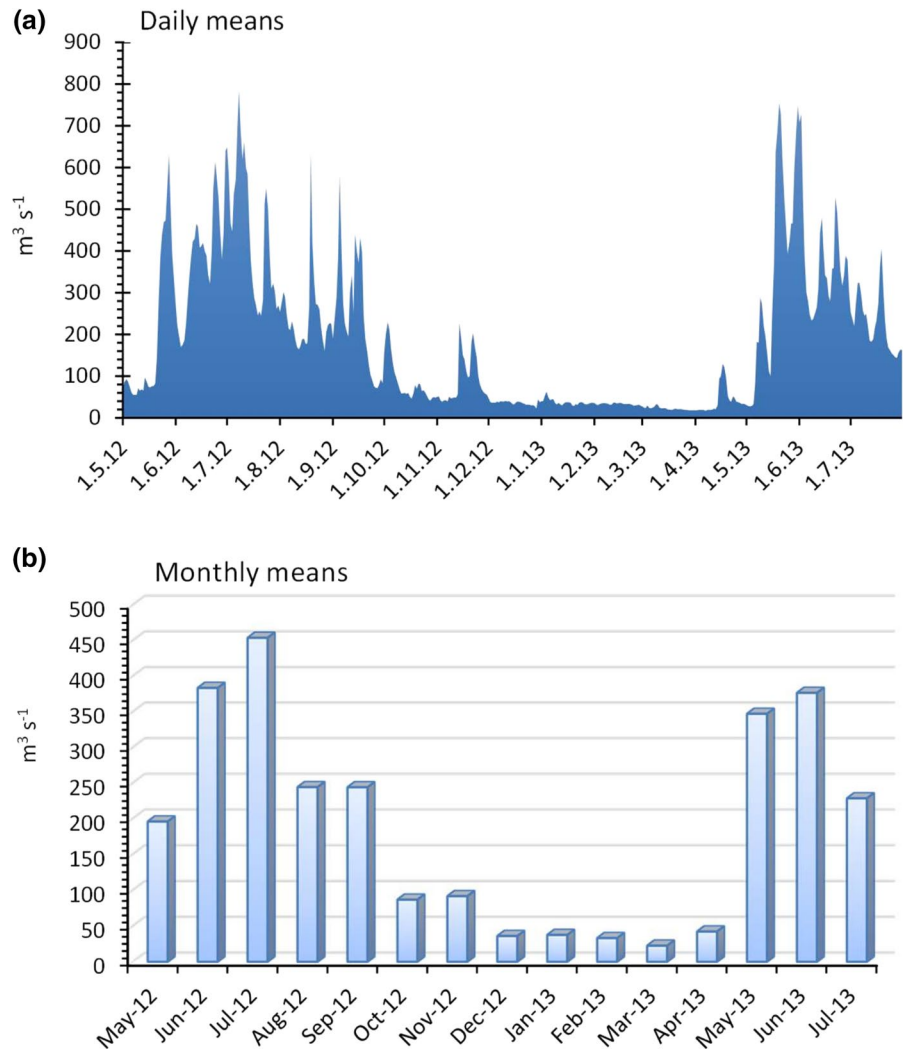


Within the 1000–1200 m depth interval oxygen values increased steadily from February to July 2013. Apparent oxygen utilization (AOU) varied between $-0.73$ mL $L^{-1}$ in July at 5 m, and 2.13 mL $L^{-1}$ in February at 1220 m.

Nutrients

Concentrations of $NO_3^-$, $Si(OH)_4$ and $PO_4^{3-}$ increased between surface and sill depth (170 m). In the basin water variations were small, with a wider range for $Si(OH)_4$ than for $NO_3^-$ and $PO_4^{3-}$ (Fig. 4a–c). In total, $NO_3^-$, $Si(OH)_4$ and $PO_4^{3-}$ ranged from 0–15.6, 0.2–17.2 and 0–1.29 µM, respectively. Concentrations of $NO_3^-$, $Si(OH)_4$ and $PO_4^{3-}$ in the surface layer (5 m) varied between 0–4.0, 0.4–4.5, 0–0.46 µM,

respectively, in the lower intermediate layer (200 m) between 9.8–13.2, 5.8–14.5, 0.79–1.13 µM, respectively, and in the lower basin layer (1220 m) between 12.6–15.6, 14.3–17.2, 1.18–1.29 µM, respectively. Maximum nutrient concentrations at 200 m occurred during late winter-early spring 2013, peaking in March. From March to July 2013 upwelling likely forced water originating at 1000 m upwards to 100 m, making this part of the water column relatively homogenous with respect to nutrients, showing $NO_3^-$, $Si(OH)_4$ and $PO_4^{3-}$ concentrations of 11 µM, 6 µM, and 0.9 µM, respectively. During winter, the $NO_3^-/PO_4^{3-}$ ratio was at its highest at 5 m while from 50 m and below it was at its lowest (Fig. 4e).

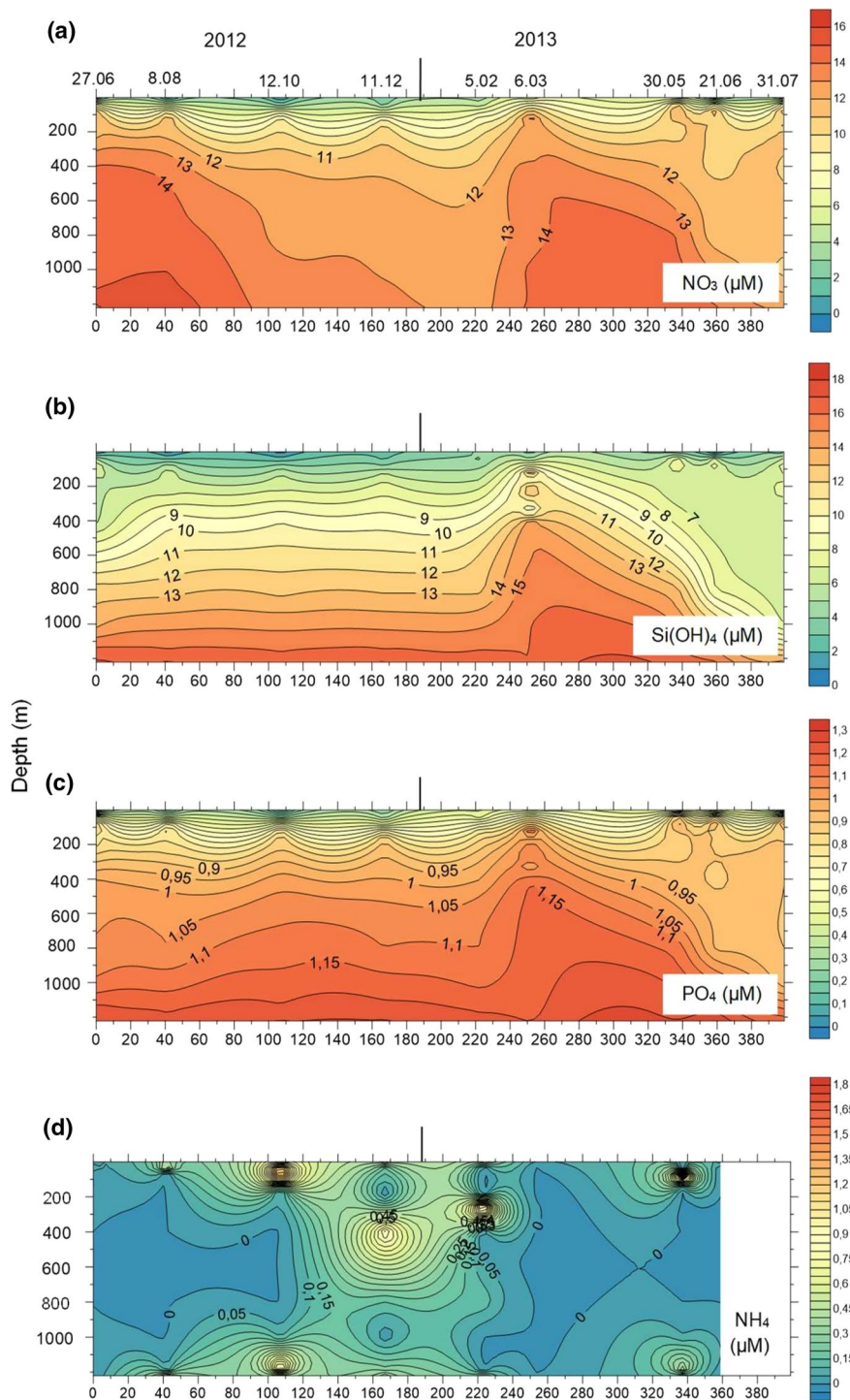$NH_4^+$ concentrations varied from 0–1.85 µM across all depths and dates (Fig. 4d) and were in

**Fig. 4** Nutrient isopleth diagrams (0–1220 m) in the Sognefjord from 27 June 2012—31 July 2013 for **a** nitrate (NO$_3$), **b** silicate (Si(OH)$_4$), **c** phosphate (PO$_4$), **d** ammonium (NH$_4$), and **e** NO$_3$: PO$_4$ at 5, 50, 200, 800 and 1220 m
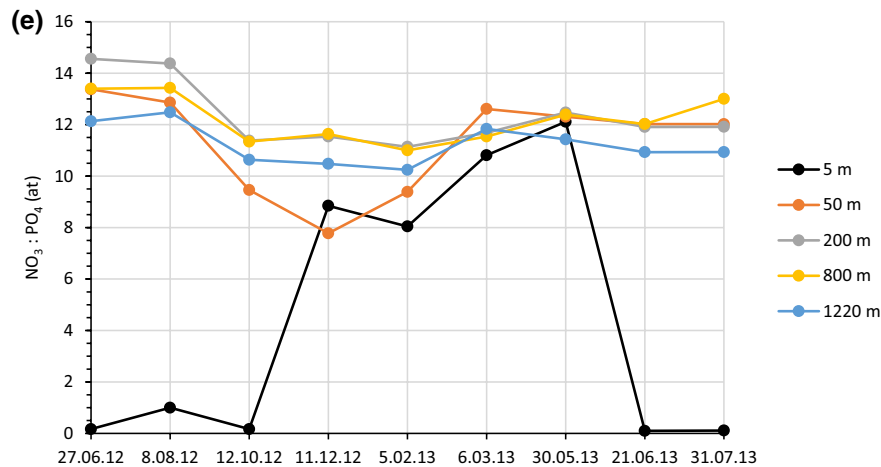
**Fig. 4** (continued)

general highest during winter. However, independent of season, high $NH_4^+$ concentrations were frequently seen in the upper layer and at some depths in the basin layer. The highest values were encountered above the sill, with 1.85 µM at 70 m in May. Below sill depth $NH_4^+$ values were $\leq 1.29$ µM, reaching 1.29 µM in February at 250 m and 1.0 µM in October at 1200 m. Notably, $NH_4^+$ was depleted over the whole water column in March.

Chlorophyll *a* fluorescence

Chl *a* fluorescence was strong around 15 m depth in June 2012, and in May–June 2013 (1.9–2.4 µg $L^{-1}$) (Fig. 5a, b). A deep chl *a* maximum layer was seen at 30 m in June 2012 (1.8 µg $L^{-1}$) and at 25 m in June 2013 (1.3 µg $L^{-1}$). Subsurface maxima were seen also in March, with a peak at 17 m depth (1.3 µg $L^{-1}$). Even if chl *a* decayed exponentially with depth (see Fig. 5b, inserted), modest levels of chl *a* were also observed below sill depth in June, ranging from 0.12–0.28 µg $L^{-1}$ within the depth interval 206–282 m.

Prokaryote, virus, and phytoplankton abundance

Prokaryote abundance was highest in the surface water during summer, ranging from approximately 2.1–13.08 × $10^5$ cells $mL^{-1}$ (Table S2). Abundance

in the intermediate water ranged between 1.49 and 3.27 × $10^5$ cells $mL^{-1}$ and in the basin water between 1.22 and 2.10 × $10^5$ cells $mL^{-1}$. Virus abundances also decreased with depth, ranging from a of 3.4–23 × $10^6$ particles $mL^{-1}$ in the surface water to 1.24–2.58 × $10^6$ particles $mL^{-1}$ in the basin water (Table S2). Seasonal variations in prokaryote and viral abundances were most pronounced in the surface water, and least in the basin water. Blooms of nanophytoplankton and picophytoplankton (including the cyanobacteria *Synechococcus* spp.) were observed in the upper layer between June–August. Elevated abundances of phytoplankton were also observed in March whereas phytoplankton biomass was low during late autumn and winter. A bloom of the coccolithophorid *Emiliania huxleyi* was observed in the upper part of the water column from May–June 2013, corresponding with the most turbid waters observed in this study.

Vertical variations in SPM elemental concentrations during an annual cycle

Value ranges for the elements C, O, N, Si, Ca, Cl, P, Fe, Mg, Na, Mn, K, Zn, S, Cu are given in Table 1 (concentrations ranging over 4 orders of magnitude). Particulate elements are presented in groups according to similarity in their overall mean concentrations (depths and dates).

**Fig. 5 a** Isopleth diagram of chl *a* (0–300 m) in the Sognefjord for the period 27 June 2012–21 June 2013 (31 July not included due to technical failure). **b** Vertical profiles of chl *a*: 0–1220 m and 0–100 m inserted. Sill depth (170 m) and depth coinciding with chl *a*=0.1 μg L$^{-1}$ (according to exponential decay equation inserted) (47.8 m) are shown by black and green dashed horizontal lines, respectively
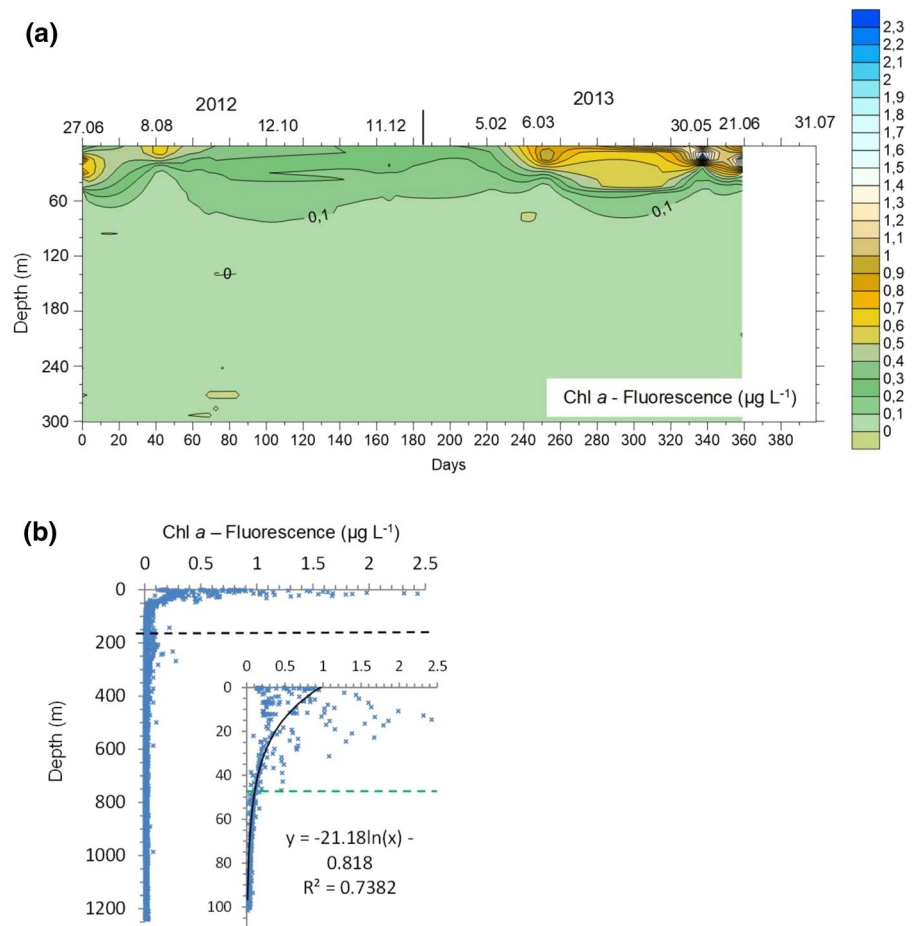


**Table 1** Maximum (max), minimum (min,) and overall means (across all dates and depths) with standard errors (SE) of seston elemental concentrations (μM) in the Sognefjord

| Element | Max (μM) | Depth (m) | Min (μM) | Depth (m) | Mean (μM) | SE (±) |
|---|---|---|---|---|---|---|
| C | 32.8737 (21.06.13) | 5 | 1.5173 (8.08.12) | 200 | 5.2747 | 0.5530 |
| O | 5.5275 (5.02.13) | 1220 | 0.0797 (8.08.12) | 200 | 1.5705 | 0.1277 |
| N | 3.7785 (21.06.13) | 5 | 0.0454 (27.06.12) | 1220 | 1.5400 | 0.0915 |
| Si | 1.4551 (5.02.13) | 1220 | 0.0702 (8.08.12) | 200 | 0.3433 | 0.0198 |
| Ca | 4.4309 (21.06.13) | 5 | 0.0699 (11.12.12) | 800 | 0.3274 | 0.0724 |
| Cl | 0.3529 (8.08.12) | 5 | 0.0465 (5.02.13) | 50 | 0.1640 | 0.0094 |
| P | 0.7247 (27.06.12) | 5 | 0.0206 (8.08.12) | 200 | 0.0953 | 0.0124 |
| Fe | 0.3404 (5.02.13) | 1220 | 0.0229 (12.10.12) | 50 | 0.0702 | 0.0041 |
| Mg | 0.2576 (5.02.13) | 1220 | 0.0286 (31.07.13) | 50 | 0.0677 | 0.0042 |
| Na | 0.1596 (5.02.13) | 1220 | 0.0252 (5.02.13) | 50 | 0.0649 | 0.0035 |
| Mn | 0.2252 (30.05.13) | 1220 | 0.0038 (27.06.12) | 50 | 0.0490 | 0.0058 |
| K | 0.1588 (5.02.13) | 1220 | 0.0040 (31.07.13) | 50 | 0.0348 | 0.0029 |
| Zn | 0.1025 (30.05.13) | 1220 | 0.0074 (12.10.12) | 1220 | 0.0319 | 0.0022 |
| S | 0.0905 (21.06.13) | 5 | 0.0063 (31.07.13) | 800 | 0.0199 | 0.0018 |
| Cu | 0.0190 (5.02.13) | 1220 | 0.0010 (5.02.13) | 50 | 0.0076 | 0.0005 |

The. Sampling was conducted at 5, 50, 200, 800 and 1220 m during 9 cruises from 27 June 2012 to 31 July 2013. Time and depth at which max, and min values occurred are also given. Elements arepresented in descending order with regard to mean concentration

## Particulate C–O–N

Particulate C and O were within the range 1.52–32.87 μM and 0.08–5.53 μM, respectively (Fig. 6, Table 1). Both had their minimum at 200 m in August, while maximum for C was at 5 m in June 2013 and for O at 1220 m in February. Values of particulate O and N were relatively low at all depths until winter 2013, when a marked increase was observed (Fig. 6). Particulate N was within the range 0.05–3.78 μM, with maximum obtained in June 2013 and minimum in June 2012. The overall means (time and depth) of particulate C, O and N were 5.28 μM, 1.57 μM and 1.54 μM, respectively (Table 1). The annual mean of particulate C, O and N at specific depths had their maxima at 5 m, with 13.92 μM, 2.39 μM and 2.13 μM, respectively (Table 2).

## Particulate Si–Ca–Cl

Particulate Si and Ca were within the range 0.07–1.46 μM and 0.07–4.43 μM, respectively (Fig. 6, Table 1). Si had its maximum at 1220 m in February and Ca at 5 m in June 2013. Si concentrations were also high in the surface layer during summer. Minimum concentrations of particulate Si and Ca were found at 200 m in August and at 800 m in December, respectively. Particulate Cl was within the range 0.05–0.35 μM and had its maximum at 5 m in August and minimum at 50 m in February (Table 1). The overall means (time and depth) of particulate Si, Ca and Cl were 0.34 μM, 0.33 μM and 0.16 μM, respectively (Table 1). As was the case for particulate C, O, and N, annual mean of particulate Si, Ca and Cl at specific depths had their maxima at 5 m with 0.51 μM, 1.12 μM and 0.21 μM, respectively (Table 2), but Si differed from Ca by having a high concentration (0.46 μM) also in the bottom layer (1220 m).

## Particulate P–Fe–Mg

Particulate P concentrations were within the range 0.02–0.72 μM and consistently low at depths beneath 5 m, with minimum at 200 m in August and a maximum at 5 m in June 2012 (Fig. 6, Table 1). Concentrations of P were also relatively high at 5 m during May–July 2013, reaching levels of 0.30–0.35 μM. Particulate Fe and Mg were within the range 0.02–0.34 μM and 0.03–0.26 μM, respectively but in contrast to P, Fe and Mg had their maximum at 1220 m in February, while minimum was encountered at 50 m in October and July, respectively. Particulate Fe achieved an even higher concentration (0.76 μM) at 250 m in February, coinciding with the bottom of the halocline (data not shown). The overall means (time and depth) of P, Fe and Mg were 0.095 μM, 0.070 μM and 0.068 μM, respectively (Table 1). As was the case for annual mean of particulate C, O, N, Si, Ca and Cl at specific depths, P had its maximum (0.25 μM) at 5 m, while Fe and Mg at 1220 m with 0.13 μM and 0.10 μM, respectively (Table 2).

## Particulate Na–Mn–K

Particulate Na, Mn and K were within the ranges 0.06–0.16 μM, 0.05–0.23 μM and 0.03–0.16 μM, respectively, all with their maximum at 1220 m, obtained in February, May, and February, respectively (Fig. 6, Table 1). Minimum for Na, Mn and K were encountered at 50 m and occurred in February, June 2012, and July, respectively. High concentrations of Mn were only found in the basin layer, where values at 1220 m exceeded the values at 800 m by a factor of 5 and the depth strata above by a factor of $\geq 10$. The overall means (time and depth) of Na, Mn and K were 0.065 μM, 0.049 μM and 0.035 μM, respectively (Table 1). Annual mean of Mn and K at specific depths had their maximum at 1220 m with 0.18 μM and 0.06 μM, respectively, while vertical differences of Na were less pronounced (Table 2).

## Particulate Zn–S–Cu

Particulate Zn, S and Cu were within the ranges 0.007–0.103 μM, 0.006–0.091 μM, 0.001–0.019 μM, respectively (Fig. 6, Table 1). Particulate S had its maximum at 5 m in June 2013, while Zn and Cu at 1220 m in May and February, respectively. However, measurements at 250 m in the lower halocline in February revealed still higher values for Zn and Cu, with 0.199 μM and 0.020 μM, respectively (data not shown). Minimum concentrations for Zn, S and Cu were found at 1220 m in October, at 800 m in July, and at 50 m in February, respectively. The overall (time and depth) mean values of Zn, S and Cu were 0.032 μM, 0.020 μM and 0.008 μM, respectively (Table 1). Annual mean of Zn and Cu at specific
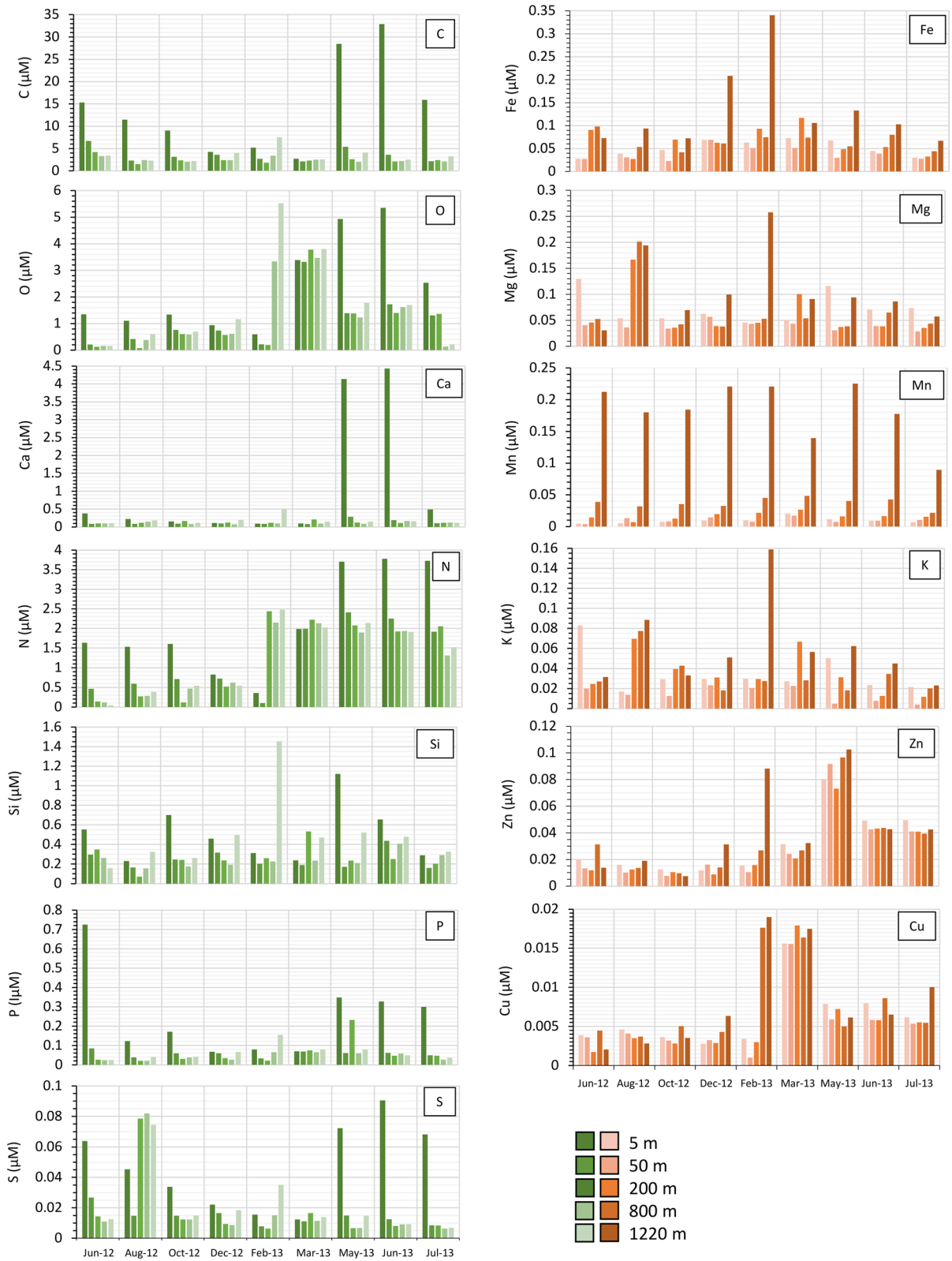
◀**Fig. 6** Variations in seston elemental concentrations (µM) in the Sognefjord from 27 June 2012 to 31 July 2013 at 5, 50, 200, 800, 1220 m. Particulate elements are presented according to similarity in their overall mean concentrations (depths and dates), those tending to have high concentrations towards the surface in the left column (green) and those towards the bottom in the right column (orange). For the clarity, standard errors are not shown, but these can be obtained from Table 1

depths showed highest concentrations in the deep basin water with 0.042 µM at 1220 m, and 0.008 µM at 800 m and 1220 m, respectively, which corresponds well with the patterns for Fe, Mg, Mn, and K (Table 2). For S, on the other hand, annual mean had its maximum at 5 m with 0.049 µM.

*Statistical analyses*

Some differences in elemental composition were observed between the different water layers (Fig. 7a), however, the dispersion of variances (betadisper) indicated that these differences were not significant ($p = 0.02$). Axis 1 of the PCoA explained 74% of the observed variability, whereas axis 2 explains 18% of the variability. The db-RDA constrained by all variables (Fig. 7b) indicated some partitioning between the surface samples and the other samples, and the surface samples also showed high dissimilarity between sampling seasons. With some exceptions, the samples from the intermediate and deeper water layers grouped together in three fractions according to sampling season: late winter (February and March), spring–summer (May, June, July) and late summer-early winter (August, October, December) (Fig. 7b). Temperature, oxygen concentration and the abundance of prokaryotes and phytoplankton appeared more closely related to the elemental composition in the surface layer than the deeper layers. Ammonium concentration appeared to be linked to the samples from August, whereas nitrite appeared to influence the samples from winter/spring that did not group in the forementioned fractions (Fig. 7b). The remaining inorganic nutrients, as well as salinity and density appeared positively correlated with PCoA axis 1, but not with any of the individual samples. The only variables that significantly affected the sample distribution were temperature, salinity and *Synechococcus* abundances (anova, $p < 0.005$).

The db-RDA constrained by microbial counts only (Fig. 7c) showed similar partitioning between the samples as in Fig. 7b, with all the constraining variables appearing to be linked to the elemental composition of the surface samples. Constraining the data with only the microbial counts gave a more pronounced seasonal partitioning between the samples obtained from the deeper layers than when all data was included (Fig. 7b). However, the only significant variable in this ordination was chl *a* fluorescence (anova, $p < 0.005$). The distribution of samples obtained from the db-RDA constrained by inorganic nutrient and oxygen concentration (Fig. 7d) appeared very similar to the ordination constrained by all variables (Fig. 7b). $NO_3^-$ was the only significant variables for this ordination (anova, $p < 0.005$).

## Discussion

We have previously shown that the bacterial community structure along a fjord-gradient in the SF was strongly influenced by allochthonous species in the surface and intermediate layers originating from freshwater runoffs and inflow from adjacent coastal waters (Storesund et al. (2017). The community composition of the deep basin water, on the other hand, showed low affiliation with adjacent water masses, and had therefore developed into a distinctive bathyal fjord microbial community characterized by low disturbance, except during episodic replacement of bottom water (Fosså and Brattegard 1990; Storesund et al. 2017). In the present study we have focused on seston element composition and stoichiometry during an annual cycle, covering the whole water column at one station in the outer part of the fjord, and the impact from microorganisms and environmental factors on the element composition.

Hydrodynamics and particle transport mechanisms

The sheltering effect from the surrounding mountains makes the water column of the fjord less exposed to mixing, and therefore stratification more likely to occur. The impact from hydroelectrical power production during winter was not very noticeable in the outer part of the fjord (Fig. 2), despite contributions of on average 248% higher freshwater outlets to the inner fjord in January–February compared to natural runoffs (Berg et al. 2017). Brackish surface water

Table 2 Annual means of seston elemental concentrations (µM) at specific depths in the Sognefjord

| Depth (m) | C (µM) | O (µM) | N (µM) | Si (µM) | Ca (µM) | Cl (µM) | P (µM) | Fe (µM) | Mg (µM) | Na (µM) | Mn (µM) | K (µM) | Zn (µM) | S (µM) | Cu (µM) |
|---|---|---|---|---|---|---|---|---|---|---|---|---|---|---|---|
| 5 | 13.9217 | 2.3924 | 2.1278 | 0.5062 | 1.1234 | 0.2111 | 0.2521 | 0.0512 | 0.0730 | 0.0893 | 0.0093 | 0.0346 | 0.0317 | 0.0485 | 0.0063 |
| ± | 1.9691 | 0.3331 | 0.2424 | 0.0558 | 0.3351 | 0.0285 | 0.0485 | 0.0034 | 0.0068 | 0.0095 | 0.0009 | 0.0046 | 0.0047 | 0.0053 | 0.0008 |
| 50 | 3.6560 | 1.1559 | 1.4259 | 0.2434 | 0.1255 | 0.1539 | 0.0563 | 0.0392 | 0.0391 | 0.0536 | 0.0103 | 0.0150 | 0.0291 | 0.0137 | 0.0060 |
| ± | 0.3196 | 0.1855 | 0.1764 | 0.0199 | 0.0142 | 0.0238 | 0.0030 | 0.0031 | 0.0018 | 0.0072 | 0.0008 | 0.0016 | 0.0053 | 0.0010 | 0.0009 |
| 200 | 2.4034 | 1.2080 | 1.5059 | 0.2647 | 0.1290 | 0.1651 | 0.0643 | 0.0662 | 0.0613 | 0.0600 | 0.0166 | 0.0445 | 0.0263 | 0.0184 | 0.0058 |
| ± | 0.1451 | 0.2514 | 0.1906 | 0.0252 | 0.0068 | 0.0202 | 0.0202 | 0.0057 | 0.0100 | 0.0073 | 0.0011 | 0.0100 | 0.0041 | 0.0054 | 0.0010 |
| 800 | 2.50899 | 1.3653 | 1.3292 | 0.2386 | 0.1065 | 0.1465 | 0.0432 | 0.0647 | 0.0483 | 0.0491 | 0.0375 | 0.0327 | 0.0344 | 0.0181 | 0.0083 |
| ± | 0.1036 | 0.2520 | 0.1742 | 0.0148 | 0.0062 | 0.0150 | 0.0037 | 0.0037 | 0.0021 | 0.0047 | 0.0016 | 0.0040 | 0.0051 | 0.0049 | 0.0012 |
| 1220 | 3.4467 | 1.8325 | 1.3696 | 0.4624 | 0.1730 | 0.1407 | 0.0638 | 0.1249 | 0.1032 | 0.0722 | 0.1818 | 0.0574 | 0.0417 | 0.0225 | 0.0078 |
| ± | 0.2982 | 0.3462 | 0.1846 | 0.0630 | 0.0200 | 0.0195 | 0.0067 | 0.0155 | 0.0132 | 0.0091 | 0.0090 | 0.0072 | 0.0063 | 0.0048 | 0.0013 |

Sampling was conducted during 9 cruises from 27 June 2012 to 31 July 2013. The selected depths represent surface water (5 m), intermediate water (50 m, 200 m) and basin water (800 m, 1220 m). Standard errors are given as (±)

was mainly observed during the snow melting season in May–July (see Figs. 2, 3), and there was a positive correlation between freshwater runoff and surface concentrations of particulate S, C, P, Mg, and Ca (Table S3), indicating influence from terrestrial sources. For the bottom layer correlations were weak and mostly negative.

The density of the inflowing water determines its intrusion depth and thereby the degree of deep-water renewal. Our data showed that the salinity of the basin water increased significantly from October and remained high until July. In February and May salinities were similar over the depth interval 200–1220 m, while in June and July the salinity was higher at 800 m than at 1220 m indicating that the inflowing AW did not reach the bottom layer (Fig. 2c). However, due to higher temperature of this saline water, the density became the same as at 1220 m (Fig. 2d, e). The general increase in salinity for the whole basin (1220–200 m) from October to December (60 days) during the inflow and upwelling of saline AW indicates ascent velocities of 17 m day$^{-1}$, which are in accordance with those for eddies (20–40 m day$^{-1}$) and coastal upwellings (17 m day$^{-1}$) (Johnson 1977; Vélez-Belchí and Tintoré 2001).

Typical sinking speeds of different types of particles in saltwater are 8.6 m day$^{-1}$ for clay (Tan et al. 2012; Sutherland et al. 2014), 10 m day$^{-1}$ for marine aggregates in Norwegian fjord water (Bach et al. 2016), and for living phytoplankton from -0.4 to > 2.2 m day$^{-1}$ (Peperzak et al. 2003; Erga et al. 2010, 2015). Neglecting horizontal advection and assuming low degree of flocculation, SPM in the form of phytoplankton would need more than 80 and 500 d to reach sill depth and fjord bottom, respectively. At greater distances from river outlets the smallest size fractions (e.g., clay) is expected to be predominant due to lower settling speeds. Clay particles at the top of the intermediate layer would need 15 d to sink from 40 to 170 m, but due to a significant horizontal transport during this residence time they could potentially be transported horizontally 13 to 65 km before being trapped within the fjord basin (see Storesund et al. 2017). Given this scenario, all clay particles being fed into the inner fjord system would be kept within the fjord basin, while bacteria and phytoplankton could be flushed out of the fjord before reaching the basin. However, inflows of AW over the sill (Fig. 1a), occurring at
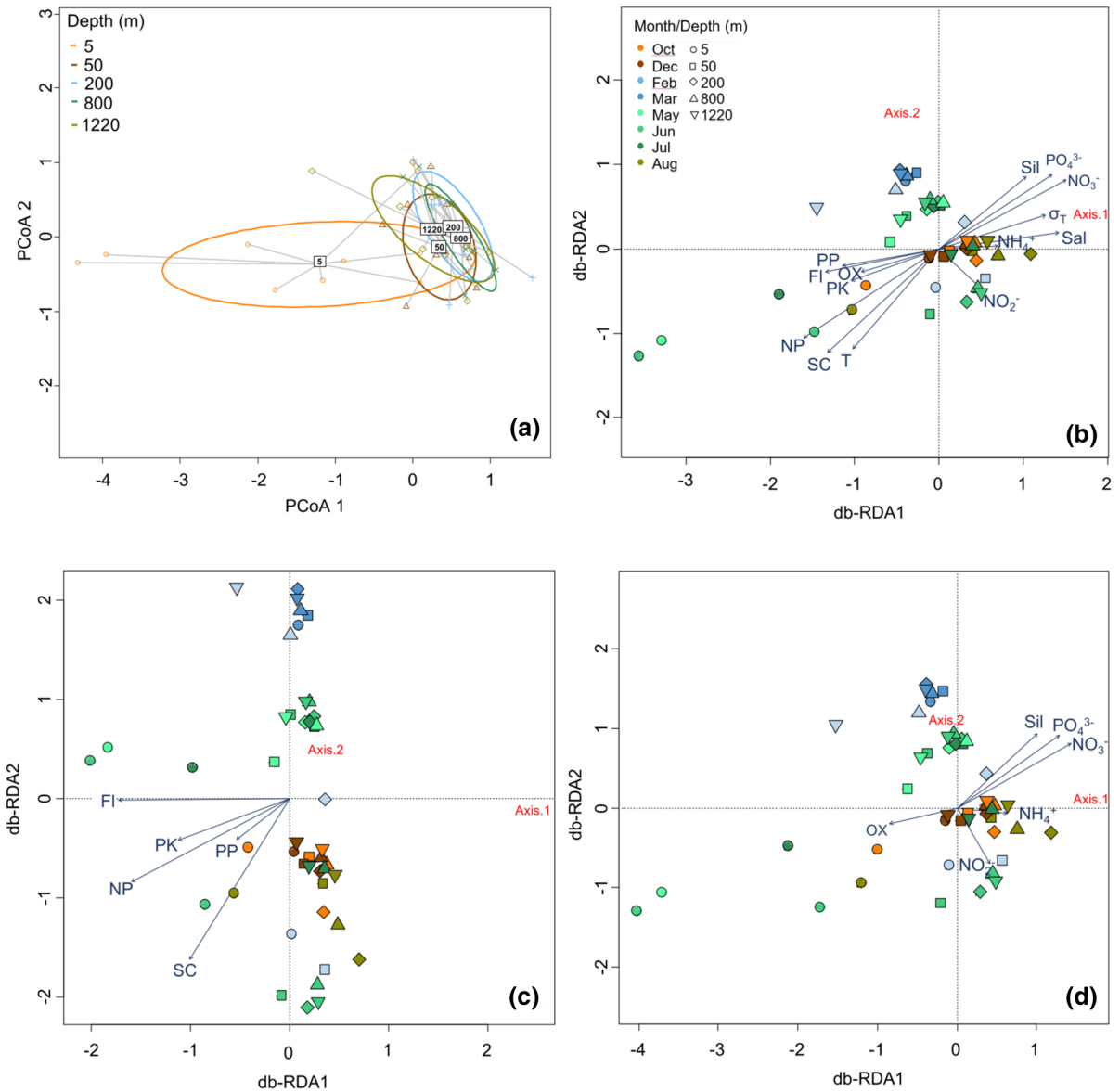
**Fig. 7 a** Principal Coordinate Analysis (PCoA) indicating difference in elemental composition between samples from different depths in the Sognefjord during the period 27 June 2012–31 July 2013. The closer the points cluster, the more similarities they have in their elemental composition **b** Distance based redundancy analysis (db-RDA) constructed from the primary and secondary PCoA axes using temperature (T), salinity (Sal), density ($\sigma_t$), $O_2$ (OX), chl *a* fluorescence (Fl), inorganic nutrients ($NO_3^-$, $NO_2^-$, $NH_4^+$, $Si(OH)_4$ (Sil), $PO_4^{3-}$) and microbial counts (Prokaryotes (PK), Nanophytoplankton (NP), Picophytoplankton (PP), *Synechococcus* (SC)) as constraints. **c** db-RDA constructed using OX, $NO_3^-$, $NO_2^-$, $NH_4^+$, Sil and $PO_4^{3-}$concentrations as constraints, and **d** db-RDA using microbial counts and chl *a* fluorescence as constraints. The orientation of the PCoA axes in the db-RDA ordinations are indicated in red

irregular intervals (Storesund et al. 2017), could lead to both import of particulate matter (PM) from offshore waters and resuspension of clay sediments by entrainment. Important in this context is the advective force generated by weak bottom currents. In the SF maximum velocity around 0.06–0.07 m s$^{-1}$ (data not shown), appeared close to the bottom during inflow periods of heavy AW.

In August and February clay/silt particles were seen on the filters from 1220 m, confirming such bottom-up circulation process.

Nutrient dynamics

Based on dissolved nutrients data (5–1220 m), linear regression gave $NO_3^-/PO_4^{3-}$, $Si(OH)_4/PO_4^{3-}$ and $NO_3^-/Si(OH)_4$ atomic ratios of 12.7, 12.5 and 0.8 respectively (Table S4), which differ slightly from the classical N:Si:P = 16:16:1 ratio often used as criteria for stoichiometric nutrient balance of diatom-dominated systems (Brzezinski 1985) (see later discussion for the importance of diatoms in the SF system). However, considering only the basin layer (200–1220 m), overall N:Si:P ratios were 8.6:28.4:1 (N/Si = 0.3). For the upper 200 m of the water column, the N:Si:P ratio was 13.5:8.1:1 (N/Si = 1.4), which is similar to previous findings at 100 m in the adjacent NCC water and at 200 m depth in the Norwegian Sea (Erga et al. 2014, 2017). This indicates a continuum in similar nutrient concentrations from offshore to inshore waters within the intermediate layer, which has a vertical extension varying from 15–200 m to 50–200 m during the year (Fig. 2a). The N/P ratio at specific depths revealed lower values in winter than spring–summer from 50 m (i.e. below euphotic zone) and downwards (Fig. 4e), indicating faster turnover for $PO_4^{3-}$ than $NO_3^-$. The strong contrast between silicate concentrations in the deep water outside (low) the sill and basin water inside (high), emphasizes the importance of fjord basins as silicate reservoirs for the united coastal regime. A similar contrast has been observed for deep water in other Norwegian fjords as well (Stigebrandt and Aure 1989). From December to March upwelling of nutrient-rich basin water reached shallower depths than 100 m (Fig. 4a–c). In July, the upwelling of AW displaced the original deep water completely, revealed by lowered silicate values over the entire water column (1000 m) during a 60-day period (Fig. 4b). This gives an ascent rate of 17 m day$^{-1}$, consistent with the speed found at an early stage of the upwelling (see above).

$NH_4^+$, an alternative N-source for growth of microbiota, showed a different variation pattern than $NO_3^-$ (Fig. 4a, d), with levels (0–1.85 μM) similar to those found in the Oslofjord (Paasche and Erga 1988), but higher than in the oligotrophic Northeast Atlantic (values ≤ 0.1 μM) (Rees et al. 2006). The depletion of dissolved $NH_4^+$ throughout most of the water column during upwelling in February–March could be due to inflow of $NH_4^+$ deprived AW, removal of $NH_4^+$ cations by adsorption onto ascending and negatively charged clay/silt particles, or complex binding within organic ligands (Van Raaphorst and Malschaert 1996; Eturki et al. 2012). In general, the N-variation patterns indicate complex $NH_4^+$ conversion processes in both the pelagic and benthic parts of the fjord, such as procaryotic ammonification, shift from ammonification to nitrification (ammonium oxidation), $NH_4^+$ adsorption to negatively charged PM, or $NH_4^+$ release from nitrogen mineralization in anoxic $MnO_2$-rich sediments (Liebes 1992; Thamdrup and Dalsgaard 2000; Winkelmann and Knies 2005; Abdulgawad et al. 2008). Local runoffs from agriculture are of minor importance in this context (http://www.vannportalen.no/sognogfjordane). Specifically, it has been found that nitrification by the bacteria *Nitrosomonas* sp. and *Nitrobacter* sp. may occur when attached to suspended inorganic particles (Diab and Shilo 1988).

Seston elemental stoichiometry: the role of microbiota and environmental factors

The seston composition could be significantly changed during transport from source to sink by interferences with freshwater runoffs/land drainage, entrainment at the interface between adjacent water masses or between bottom water and sediments, and coastal-fjord water exchanges (Storesund et al. 2017). Among the highlighted anthropogenic impacts of the SF ecosystem are freshwater regulations related to extensive hydropower production (Myksvoll et al. 2014), aluminum plants (smelters), ship traffic, fish farms and small- and medium-sized sewage treatment stations with low degree of treatment (Manzetti and Stenersen 2010). Contribution from aerosols should also be considered as these particles are often associated with environmental contamination (Cáceres et al. 2019).

Microorganisms are responsible for primary production, and bacterial degradation of organic material affects both the abundance of dissolved organic matter and the elemental composition of SPM. Bacteria and different groups of microalgae in the SF displayed common bloom patterns, with high cell numbers in the surface water during May,

June and July compared to other months and depths (Table S2). The amount of phytoplankton, represented by chl *a*, achieved an annual average of 0.9 and 0.7 μg L$^{-1}$ at 0 and 5 m, respectively (Fig. 5b, inserted). This compares well with another western Norwegian fjord, the Samnangerfjord, where the annual average was 1 μg L$^{-1}$ at 5 m and an overall POC/chl *a* ratio of 81 was obtained (n = 288) (Erga et al. 2005). Using this ratio on the SF data, we find that microalgae on an annual basis may contribute with 4.7 μM C of the total particulate carbon (13.9 μM) at 5 m (Table 2), meaning that 66% of the particulate C at 5 m is non-algal.

The composition of particulate elements showed larger differences between sampling months at the surface than in the deeper water masses (Fig. 7a, b), and appeared to be influenced by abundance of microorganisms and photosynthetic activity (Fig. 7b, c), emphasizing the intrinsic link between elemental composition of SPM, abundances of dissolved organic matter and microorganisms in the marine environment. Elemental composition in the different samples also differentiated between the different sampling depths, however, this was not statistically significant. When all variables were considered, the sample composition was highly linked to salinity, temperature, and the abundance of *Synechococcus* sp. (Fig. 7b). The notable difference in the deeper layers between samples from late spring and summer in elemental composition compared to other samples was probably linked to the microbial biomass (Fig. 7c), whereas the differences observed in the upper layers could be linked to photosynthesis (indicated by chl *a* concentration). Sinking particles at that time was likely composed partly of dead or dying microalgae in addition to inorganic runoffs from land. Lower concentrations for several of the major seston elements at greater depths during an annual cycle (Fig. 6), may be due to the decomposition and dilution of particles in deeper strata, or flushing out of the fjord before entering the basin layer (cf. 4.1), if sinking particles stay in the water column. For bigger particles/aggregates with high sinking speeds, settling on the bottom may also occur.

The composition of dissolved elements (NO$_3^-$–N, Si(OH)$_4$-Si, PO$_4^{3-}$-P) seemed to be mainly influenced by depth, as well as seasonality in the surface layer (Fig. 7b,d), possibly linked to consumption of these elements by microorganisms in the upper water masses, and regeneration in the deeper water masses. Competition for nutrients between prokaryotes and phytoplankton, in addition to viral lysis and grazing, significantly affects the microbial community structure (Weinbauer et al. 2007; Chow et al. 2013; Pree et al. 2017). Viral lysis could be responsible for a daily turnover of approximately 20% of marine microbial biomass (Suttle 2007). Therefore, the high viral counts in SF surface waters (Table S2) could indicate high lysis rates of prokaryotes and/or microalgae.

Stratification and seasonality have significant impacts on prokaryote abundances in marine environments (Gilbert et al. 2012; Cram et al. 2015). Mineral and organic nutrient inputs during the growth season (spring/summer) come primarily from land run-offs and freshwater discharges (Gutiérrez et al. 2015). The dynamics of microbial communities along the fjord-gradient is influenced, directly through the introduction of microbial communities in freshwater runoffs, or indirectly through the input of mineral and organic nutrients that stimulate internal competition and growth (Storesund et al. 2017). This is in accordance with the current temporal study where fluctuations in the microbial biomass was linked to seasonality and depth in the fjord (Fig. 7), and in the case of surface microbiota to the large freshwater runoffs during snow melting, while elemental composition of SPM was related to upwelling as well as seasonality, depth, and freshwater inflows. High AOU values, showing ≥ 1.8 mL L$^{-1}$ close to the bottom at all dates, and ≥ 1.3 mL L$^{-1}$ in the lower pycnocline (100–150 m) during spring–summer (Table S1), indicate significant aerobic microbial activity connected with decomposition and remineralization of settled organic matter (e.g., nitrification). It is also supported by high levels of oxygen relative to the other elements captured in seston biomass in the basin water (800–1220 m) (Table 3).

The SPM elemental composition in February at most depths differed notably from the other samples (Fig. 7b), most likely connected with an ongoing upwelling of deep water (Fig. 2a, c), which in February resulted in resuspension and elevated values of all particulate elements at 1220 m (Fig. 6). Special for particulate N, Zn and Cu, however, was high concentrations within the basin layer from February-July when repeated upwellings occurred, indicating an impact on elemental composition from the underlying sediments.

**Table 3** Time averages of seston elemental stoichiometry relative to phosphorus (P) at specific depths in the Sognefjord (see Table 2)

| Depth (m) | Stoichiometric formulas of seston elements (molar) | C/N |
|---|---|---|
| 5 | $C_{55}N_{8.4}P_1Si_{2.0}Ca_{4.5}O_{9.5}Fe_{0.20}Mn_{0.04}Zn_{0.13}S_{0.19}Cu_{0.02}$—$Cl_{0.84}Na_{0.35}Mg_{0.29}K_{0.14}$ | 6.5 |
| 50 | $C_{65}N_{25}P_1Si_{4.3}Ca_{2.2}O_{21}Fe_{0.70}Mn_{0.18}Zn_{0.52}S_{0.24}Cu_{0.11}$—$Cl_{2.7}Na_{0.95}Mg_{0.69}K_{0.27}$ | 2.6 |
| 200 | $C_{37}N_{23}P_1Si_{4.1}Ca_{2.0}O_{19}Fe_{1.0}Mn_{0.26}Zn_{0.41}S_{0.29}Cu_{0.09}$—$Cl_{2.6}Na_{0.93}Mg_{0.95}K_{0.69}$ | 1.6 |
| 800 | $C_{58}N_{31}P_1Si_{5.5}Ca_{2.5}O_{32}Fe_{1.5}Mn_{0.87}Zn_{0.80}S_{0.42}Cu_{0.19}$—$Cl_{3.4}Na_{1.1}Mg_{1.1}K_{0.76}$ | 1.9 |
| 1220 | $C_{54}N_{21}P_1Si_{7.2}Ca_{2.7}O_{29}Fe_{2.0}Mn_{2.8}Zn_{0.65}S_{0.35}Cu_{0.12}$—$Cl_{2.2}Na_{1.1}Mg_{1.6}K_{0.90}$ | 2.6 |
| Mean | $C_{55}N_{16}P_1Si_{3.6}Ca_{3.4}O_{16}Fe_{0.74}Mn_{0.51}Zn_{0.33}S_{0.21}Cu_{0.08}$—$Cl_{1.7}Na_{0.68}Mg_{0.71}K_{0.37}$ | 3.4 |

Sampling was conducted during 9 cruises from 27 June 2012 to 31 July 2013. The overall mean (all dates and depths) is at the bottom. For clarity, elements representing the major ions of seawater are separated from the other elements of the stoichiometric equation

Particulate C/P, N/P, and C/N atomic ratios across dates and depths, varied between 11–162, 1.8–116, and 0.8–75, respectively, with maximum and minimum both encountered at 200 and 1220 m (data not shown). Such large value ranges in C:N:P stoichiometry point towards complex causal relationships, not only concerning source or origin, such as organic/inorganic, limnic/marine, terrestrial/lithogenic, aerosol, and anthropogenic, but also the extent of microbial activity, geochemical/geophysical processes, and elemental turnover at different depths. To unravel systematic differences between water layers with respect to seston elemental stoichiometry, we used annual averages for each element at all depths (Table 3). At 5 m where phytoplankton contributed with 34% of the total particulate C (see above), this resulted in a C:N:P ratio of 55:8.4:1 (C/N = 6.5), which corresponds well with values for the Raunefjord (Erga et al. 2017) and Boknafjord (Erga 1989), both being situated upstream in the NCC relative to the SF (Fig. 1). It is also similar to the C:N:P = 60:7:1 of soil microbiota (Cleveland and Liptzin 2007), to the C:N:P = 50:10:1 of native aquatic and cultured bacteria (Fagerbakke et al. 1996), and is concurrent with the conclusion of Storesund et al. (2017), stating that the upper layer in the SF is influenced by bacterial communities originating from terrestrial runoffs. However, below euphotic zone there was a strong decrease in annual means of C and P, but only a modest decrease in N (Table 2), enhancing N:P ratios to 21–31:1, and reducing C:N ratios to 1.6–2.6:1 along the depth range 50–1220 m (Table 3). A similar but more distinguished trend occurred for the C:O ratio decreasing successively from 5.8:1 at 5 m to 3.1:1 at 50 m, and levels around 1.8–1.9:1 below sill depth (Table 3). Native bacteria from the Raunefjord were found to have C:O ratios within the range 2.8–5.1:1 (Fagerbakke et al. 1996).

Interestingly we found that the depletion of $NH_4^+$ over the whole water column during upwelling in March (Fig. 4) coincided with evenly distributed and high particulate N, and low particulate C and P (Fig. 6), resulting in a mean water column (5–1220 m) C:N:P ratio of 34:30:1 (C/N = 1.1) (data not shown). However, $NO_3^-$ was the only inorganic nutrient significantly linked to the composition of particulate elements in the water column (Fig. 7d) but considering the complex relationships between $NH_4^+$ and $NO_3^-$, and clay particles (Cho et al. 2010), there is reasons to believe that the amount of inorganic N present in the fjord could influence the C:N ratio. This corresponds well with the findings of Winkelmann and Knies (2005), who concluded that low C:N ratios (but higher than in our study) of marine surface sediments along the coast of Spitsbergen could be due to high inorganic N (70% of the total N). Low C:N ratios have also been reported from marine surface waters of the Canadian Arctic under the dominance of heterotrophic microbes (Crawford et al. 2015). Also, high P concentrations relative to C is characteristic for aquatic bacteria (Chrzanowski and Kyle 1996). Consequently, in our study, none of the particulate C:N:P annual means at specific depths (Table 3) were close to the oceanic Redfield ratio (106:16:1). When averaging over both time and depth, however, the particulate N:P ratio became equal to Redfield (16:1), while the C:P and C:N ratios only reached 55:1 and 3.4:1, respectively (Table 3). Together, these facts suggest contribution from heterotrophic microbes, faster microbial decomposition of C and P than N, and the

presence of N enriched inorganic particulate matter, such as clay. It could also be due to inorganic particle formation mechanisms related to redox and N-transformations processes at the sediment–water interface.

Particulate elements, sorted according to concentration, can roughly be grouped into surface: C–O–N–Si–Ca–Na–Cl–P–S and bottom: Fe–Mg–Mn–K–Zn–Cu affiliation (Fig. 6). C-Ca-P-S tended to be negatively correlated with salinity and positive with temperature (Fig. 8, shown for C and S), while Fe–Mn–Mg–K was not correlated but showed highest concentrations at salinities and temperatures typical for AW (Fig. 8, only shown for Fe). O–N–Si–Zn–Cu concentrations, on the other hand, seemed to be high in both AW and colder/warmer brackish water, and consistently low for salinities between 30 and 33 (Fig. 8, shown for N, Si and Cu). Concentrations of particulate Na and Cl were independent of salinity, while weakly positive correlated with temperature (data not shown). Based on mean values of particulate Na and Cl a molar Na/Cl ratio of 0.4 is obtained (Table 1), which is lower than for sea-salt (0.85), but agrees well with marine bacteria from the Raunefjord, where the ratio varied between 0.1 and 0.6 (Heldal et al. 2012).

Elements in the stable bottom layer (800–1220 m) had higher numbers of strong correlations ($r^2$) than at shallower depths, 16 with $r^2 \geq 0.9$ and 66 with $0.4 \leq r^2 < 0.9$ (Table 4), suggesting strong connection with microbial communities and sediments (Storesund et al. 2017). The upper layer (5–50–200 m), on the other hand, is exposed to rapid shifts in environmental conditions including horizontal advection, thereby giving the microbial community less time to degrade available particulate matter, and consequently low correlation between elements, $r^2 \geq 0.9$ only for C–Ca, C–S and Mg–Cl (Table 4). However, the high correlation between Si- and Ca–Mg–Na–K, indicates an additional contribution from the inorganic/ inert fraction of the SPM, including clay (Barton and Karathanasis 2002; Barrón and Torrent 2013). Taking all depths into account, it emerges that the strongest elemental correlations $r^2 \geq 0.9$ were obtained for C–Ca and C–S, probably related to calcite ($CaCO_3$) and organosulfur producing microorganisms, such as coccolithophorids with $CaCO_3$ coccoliths and dimethylsulfoniopropionate (DMSP) metabolism, other types of phytoplankton

and bacteria with DMSP metabolism, and particulate sulfur-containing lipids (Gašparović et al. 2018; Gebser et al. 2020). In accordance with this Ca was also correlated with the organic elements O, C, N, P ($r^2 \geq 0.43$), and S ($r^2 \geq 0.71$). The tendency of high correlations between S and the trace metals Fe, Cu and Zn (all taking part in red-ox reactions) in the basin water (Table 4) could be caused by release of metal sulfide particles from the anoxic clay/organic sediments at the bottom (Skei et al. 1996).

Particulate Si had its maximum at 1220 m, but also high values at 5 m occurred during spring–summer both years, while Ca was high only at 5 m during summer 2013, and relatively low at depths below (Fig. 6, Table 1). Diatom blooms are major contributors to the annual primary production in Norwegian fjords and based on previous studies (Erga and Heimdal 1984; Paasche and Erga 1988; Erga 1989; Erga et al. 2005) it can be calculated that diatom and coccolithophorid (dominated by *Emiliania huxleyi*) blooms in Norwegian fjords with cell numbers $> 10^6$ cells $L^{-1}$, periodically can contribute with $> 1.3$ μM of particulate Si and $> 0.4$ μM of particulate Ca (Paasche 1980, 2002; Erga 1989; Fagerbakke et al. 1994). These high levels compared with total elemental Si and Ca values (Fig. 6) emphasize the importance of marine silicate- and carbonate producing microbiota as potential sources of particulate Si and Ca in fjord sediments (Aarseth 1997; Paetzel and Dale 2010; Faust et al. 2017). The relatively close relationship between Si and the organic components O, C, N, P ($r^2 \geq 0.41$) (Table 4) point towards a significant contribution from biogenic silicate. However, as biogenic silicate ($SiO_2 \cdot n(H_2O)$) dissolves slowly, Si is regenerated at greater depths than N and P (Liebes 1992). When averaging over time and depth we obtained a particulate Si:P ratio of 3.6:1 (Table 3), which compares well with earlier findings in the Raunefjord (Erga et al. 2017). Our data showed a high correlation between Si and -Mg, -K, -Ca, -O in the basin water (800–1220 m), $r^2 \geq 0.71$, compared with the upper part of the water column (5–200 m) where correlations were lower, $r^2 \geq 0.29$ (Table 4), which fits well with the vertical distribution of clay particles (Mg-, K-, Ca-$SiO_2$), quantitatively the most important terrestrial particles drained into the western Norwegian fjords (Aarseth 1997).

The annual means of particulate Fe, Mn, Mg and K stoichiometry relative to P increased steadily with

**Fig. 8** Relationship between particulate elements (µM) and salinity, and temperature (°C) in the Sognefjord during the period 27 June 2012 – 31 July 2013. Vertical lines in the bottom panel, dashed for salinity and dotted for temperature, indicate value range for the different water types: Atlantic water (AW); salinity ≥ 35, Coastal water (CW); salinity 33–34.99, Fjord water (FW); salinity 30–33, and Brackish fjord water (BFW); salinity < 30. Due to overlap in the temperature range for the various water types, only the range for AW; 7.34–8.20 °C is shown
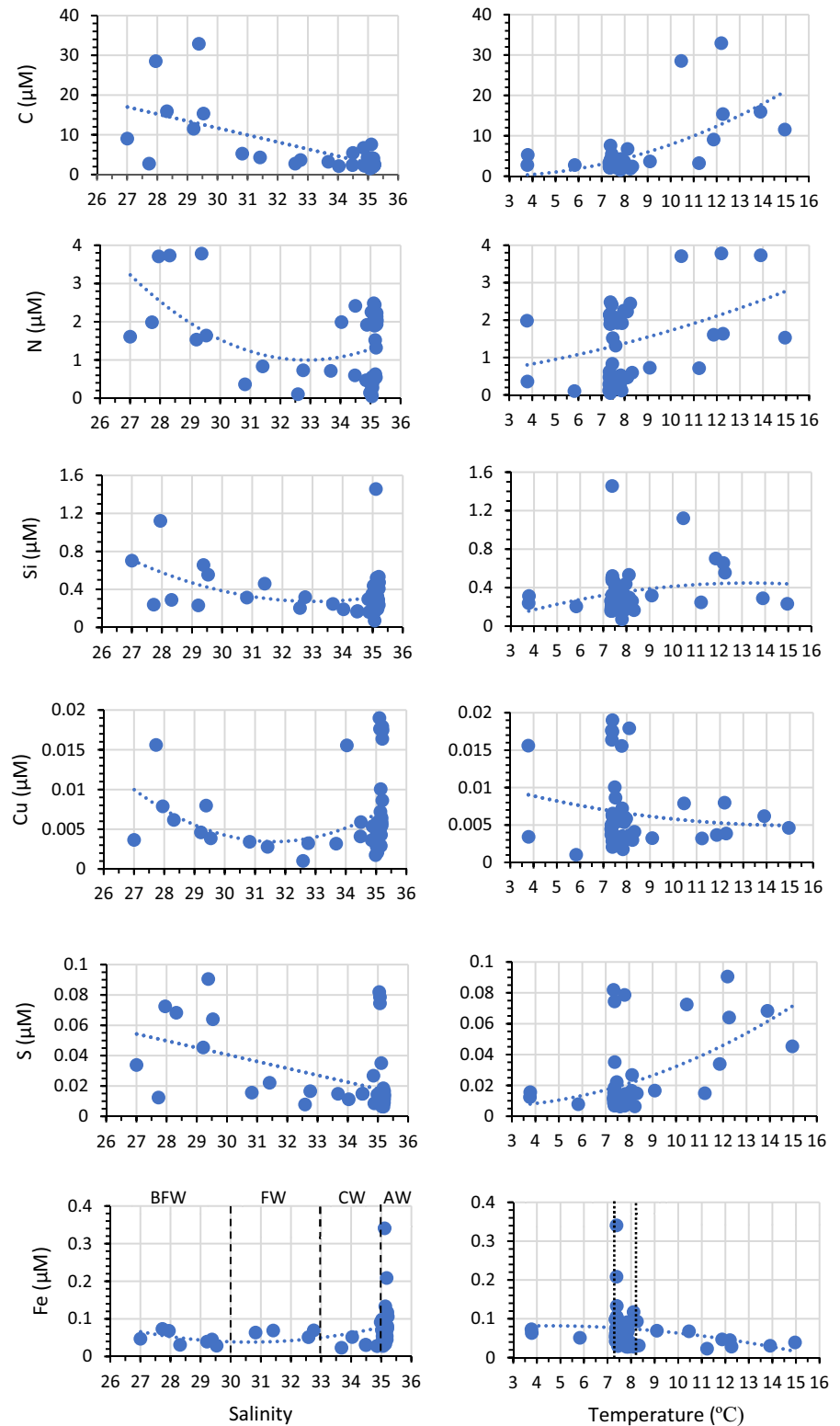
**Table 4** Correlation matrixes of different elements (mol) in seston from upper layer (5–50-200 m) (n = 27), bottom layer (800–1220 m) (n = 17), and whole water column (5–50–200–800–1220 m) (n = 44) in the Sognefjord from June 2012 to July 2013

Upper layer (5–50–200 m)

|    | C | N | P | Si | Ca | O | Fe | Mn | Zn | S | Cu | Cl | Mg | Na | K |
|----|---|---|---|----|----|---|----|----|----|---|----|----|----|----|---|
| C | 1.00 | | | | | | | | | | | | | | |
| N | **0.61** | 1.00 | | | | | | | | | | | | | |
| P | **0.70** | **0.45** | 1.00 | | | | | | | | | | | | |
| Si | **0.75** | **0.41** | **0.54** | 1.00 | | | | | | | | | | | |
| Ca | <u>0.92</u> | **0.61** | **0.46** | **0.73** | 1.00 | | | | | | | | | | |
| O | **0.67** | **0.79** | **0.40** | **0.57** | **0.74** | 1.00 | | | | | | | | | |
| Fe | − 0.19 | − 0.19 | − 0.31 | 0.16 | − 0.03 | 0.03 | 1.00 | | | | | | | | |
| Mn | − 0.35 | 0.05 | − 0.37 | − 0.14 | − 0.14 | 0.16 | **0.78** | 1.00 | | | | | | | |
| Zn | **0.41** | **0.73** | 0.28 | 0.21 | **0.46** | **0.52** | − 0.26 | − 0.05 | 1.00 | | | | | | |
| S | <u>0.96</u> | **0.59** | **0.79** | **0.70** | **0.79** | **0.62** | − 0.23 | **− 0.40** | 0.30 | 1.00 | | | | | |
| Cu | 0.05 | **0.49** | 0.05 | 0.11 | 0.15 | **0.74** | 0.22 | **0.49** | 0.28 | 0.06 | 1.00 | | | | |
| Cl | 0.31 | 0.05 | 0.30 | **0.49** | 0.22 | 0.15 | 0.12 | − 0.16 | − 0.03 | **0.41** | − 0.01 | 1.00 | | | |
| Mg | **0.61** | **0.37** | **0.75** | **0.74** | **0.48** | **0.51** | 0.25 | 0.02 | 0.10 | **0.69** | 0.26 | **0.53** | 1.00 | | |
| Na | **0.51** | 0.21 | **0.62** | **0.66** | 0.33 | 0.27 | 0.07 | − 0.23 | 0.04 | **0.63** | 0.04 | <u>0.89</u> | **0.77** | 1.00 | |
| K | 0.12 | 0.07 | **0.52** | 0.29 | 0.08 | 0.15 | 0.27 | 0.24 | 0.12 | 0.16 | 0.21 | 0.32 | **0.52** | **0.47** | 1.00 |

Bottom layer (800–1220 m)

|    | C | N | P | Si | Ca | O | Fe | Mn | Zn | S | Cu | Cl | Mg | Na | K |
|----|---|---|---|----|----|---|----|----|----|---|----|----|----|----|---|
| C | 1.00 | | | | | | | | | | | | | | |
| N | **0.40** | 1.00 | | | | | | | | | | | | | |
| P | **0.82** | **0.71** | 1.00 | | | | | | | | | | | | |
| Si | **0.71** | **0.51** | <u>0.85</u> | 1.00 | | | | | | | | | | | |
| Ca | **0.71** | **0.43** | **0.83** | <u>0.99</u> | 1.00 | | | | | | | | | | |
| O | **0.61** | *0.77* | 0.89 | **0.71** | **0.67** | 1.00 | | | | | | | | | |
| Fe | <u>0.94</u> | **0.39** | **0.77** | **0.57** | *0.56* | **0.56** | 1.00 | | | | | | | | |
| Mn | 0.18 | − 0.06 | 0.25 | **0.45** | *0.45* | 0.13 | *0.03* | 1.00 | | | | | | | |
| Zn | **0.79** | **0.61** | *0.72* | **0.49** | 0.44 | **0.48** | 0.84 | − 0.06 | 1.00 | | | | | | |
| S | <u>0.95</u> | 0.37 | <u>0.86</u> | **0.71** | 0.71 | 0.69 | <u>0.93</u> | 0.19 | **0.71** | 1.00 | | | | | |
| Cu | **0.60** | **0.75** | **0.80** | **0.55** | 0.52 | <u>0.94</u> | 0.59 | − 0.10 | **0.46** | 0.66 | 1.00 | | | | |
| Cl | 0.05 | − 0.17 | 0.12 | 0.08 | *0.07* | 0.05 | *0.19* | − 0.05 | 0.04 | 0.27 | − 0.01 | 1.00 | | | |
| Mg | **0.75** | **0.49** | <u>0.89</u> | <u>0.99</u> | <u>0.97</u> | **0.74** | *0.63* | *0.46* | 0.50 | 0.78 | **0.59** | 0.16 | 1.00 | | |
| Na | **0.75** | 0.30 | *0.80* | **0.84** | **0.81** | 0.59 | 0.69 | 0.35 | *0.57* | 0.82 | 0.46 | 0.53 | <u>0.88</u> | 1.00 | |
| K | **0.70** | **0.42** | <u>0.85</u> | <u>0.96</u> | <u>0.95</u> | 0.72 | 0.55 | 0.50 | *0.43* | 0.74 | 0.54 | 0.19 | <u>0.97</u> | <u>0.87</u> | 1.00 |

Whole water column (5–50–200–800–1220 m)

|    | C | N | P | Si | Ca | O | Fe | Mn | Zn | S | Cu | Cl | Mg | Na | K |
|----|---|---|---|----|----|---|----|----|----|---|----|----|----|----|---|
| C | 1.00 | | | | | | | | | | | | | | |
| N | **0.55** | 1.00 | | | | | | | | | | | | | |
| P | **0.72** | **0.45** | 1.00 | | | | | | | | | | | | |
| Si | **0.55** | **0.42** | **0.43** | 1.00 | | | | | | | | | | | |
| Ca | <u>0.91</u> | **0.54** | **0.48** | **0.50** | 1.00 | | | | | | | | | | |
| O | **0.53** | **0.76** | **0.38** | **0.64** | **0.56** | 1.00 | | | | | | | | | |
| Fe | 0.05 | 0.14 | − 0.01 | **0.45** | − 0.03 | **0.38** | 1.00 | | | | | | | | |
| Mn | − 0.16 | − 0.05 | − 0.15 | 0.30 | − 0.10 | 0.13 | 0.27 | 1.00 | | | | | | | |

**Table 4** (continued)

| Whole water column (5–50–200–800–1220 m) | | | | | | | | | | | | | | |
|---|---|---|---|---|---|---|---|---|---|---|---|---|---|---|
| Zn | 0.25 | **0.56** | 0.18 | **0.40** | 0.20 | **0.48** | **0.71** | 0.15 | 1.00 | | | | | |
| S | <u>0.95</u> | **0.54** | **0.79** | **0.57** | **0.77** | **0.56** | 0.17 | − 0.12 | 0.27 | 1.00 | | | | |
| Cu | 0.04 | **0.52** | 0.06 | **0.37** | 0.07 | **0.82** | **0.52** | 0.18 | **0.45** | 0.12 | 1.00 | | | |
| Cl | 0.30 | 0.00 | 0.29 | 0.29 | 0.22 | 0.09 | 0.04 | − 0.14 | − 0.05 | **0.40** | − 0.06 | 1.00 | | |
| Mg | 0.34 | **0.35** | **0.42** | **0.88** | 0.24 | **0.62** | **0.60** | **0.47** | **0.44** | **0.46** | **0.52** | 0.24 | 1.00 | |
| Na | **0.46** | 0.24 | **0.54** | **0.74** | 0.28 | **0.41** | **0.43** | 0.16 | 0.33 | **0.61** | 0.24 | **0.74** | **0.77** | 1.00 |
| K | 0.12 | 0.18 | **0.39** | **0.66** | 0.06 | **0.43** | **0.47** | **0.42** | **0.35** | 0.22 | **0.43** | 0.21 | **0.80** | **0.65** | 1.00 |

Regressions values are given as $r^2$, bold shadowing means $r^2 \geq 0.4$ and underline $r^2 \geq 0.9$. Significance levels are 5% and based on Two-tailed P values ($P < 0.05$). Values not significant on a 5% level ($P > 0.05$) are written in italic

depth from 5 to 1220 m depth (Table 3), which indicates a deep-water enrichment of these elements. The observed annual averages of K (0.015–0.057 μM) and Mg (0.039–0.103 μM) through the water column (Table 2) are within the range of other western Norwegian fjords (Price and Skei 1975; Erga et al. 2017). K and Mg play an important role in osmoregulation of marine archaea and bacteria (Martin et al. 1999; Heldal et al. 2012). We found an overall stoichiometric relationship for K:Mg:P of 0.37:0.71:1, which is approximately 10 times higher than values measured in the eastern tropical North Atlantic (Lam et al. 2012), indicating a strong contribution from terrigenous materials in the fjords. In acidic soil, which is very common in the Norwegian coastal landscape, conditions are known to facilitate exchange of $K^+$, $Ca^{2+}$ and $Mg^{2+}$ (Behera and Shukla 2014). Annual means of particulate Si increased by depth below sill due to sinking diatom frustules and clay particles. The strong increase in Mn concentrations towards the bottom (Fig. 6, Table 2), could be due to resuspension of clay particles and $MnO_2$ rich sediments driven by advection. Another possibility is Mn reduction in the sediments, followed by diffusion of $Mn^{2+}$ and reoxidation in bottom waters, consistent with relatively constant and high Mn concentrations, and elevated Mn/Fe ratios in bottom water. According to Vandieken et al. (2012), such sediments are common in Skagerrak, and contain acetate-oxidizing manganese-reducing bacteria. Our value range of Mn, 4–225 nM, compares well with that of SPM in the shallow southern North Sea, which is under influence of large riverine discharges (Nolting 1986).

Both particulate Cu and Zn were highest in the basin layer (Fig. 6, Table 2). Again, the binding properties of clay particles, known to adsorb both Cu and Zn (Sdiri et al. 2014), could explain the higher levels in the SF. However, averaging over an annual cycle at all depths, the stoichiometric relationships of seston Cu and Zn relative to P show a less pronounced pattern regarding vertical variations (Table 3). Relative high ratios also above sill depth point towards release from anthropogenic sources, which is consistent with previous findings of riverine discharges of Cu and Zn into Norwegian coastal waters (Skarbøvik et al. 2017). In addition, Cu is used as an antibacterial agent in aquaculture (Grefsrud et al. 2018), which is common in the SF.

Conclusions

Large freshwater discharges during snow melting in May–July led to a more brackish upper layer, which together with strong out-fjord winds strengthened the estuarine circulation. Below sill depth (170 m), variations in salinity and temperature were small, with Atlantic water (AW) (salinity ≥ 35.00) dominating and temperatures ≥ 7.33 °C at all depths, and oxygen saturation values never lower than 68.2% (February at 1220 m), revealing adequate supply of oxygen rich AW. Replacement of bottom water with offshore AW was driven by wind regulated upwelling, in June-July 2013 reaching depths shallower than 50 m. Conditions for recycling of Si appeared to be favourable within the fjord basin (200–1220 m), revealed by a nutrient N:Si:P (molar) ratio of 8.6:28.4:1 (N/Si = 0.3), a factor of 6 lower N/Si ratio than in adjacent offshore AW. Microbiota constituted an important part of the seston, showing a close connection between prokaryote and viral abundances, with

seasonal variations most pronounced in the surface water and least in the basin water. Fluctuations in the microbial biomass was linked to seasonality and depth, but also associated with freshwater-terrestrial inflows. In addition to these drivers, elemental composition of seston could be linked to upwelling of bottom water and terrestrial inputs. In general, the relationship between abundance of microorganisms and particulate elements appeared to be stronger than with dissolved elements. High concentrations of particulate C–O–N–Si–Ca–Cl–Na–P–S and Fe–Mg–Mn–K–Zn–Cu were found most frequently towards the surface and bottom layer, respectively. Irrespective of concentrations there were much higher numbers of strong correlations between elements in the bottom layer than the surface layer due to stable conditions at depth, while above sill there was rapid shifts in environmental conditions. None of the particulate C:N:P (molar) annual means at specific depths were close to the classic Redfield ratio (106:16:1). At 5 m the annual means of particulate N/P and C/N were 8.4 and 6.5, respectively, while at depth (50–1220 m) N/P were on scale 3 times higher (21–31) and C/N 3 times lower (1.6–2.6), suggesting alternative N-sequestration mechanisms. High correlations between Si- and C-N-P-Mg–K-Ca-O below sill indicate contribution from both clay particles and diatoms. Overall high correlation between Ca-C and S-C were likely related to calcite ($CaCO_3$) and organosulfur producing microorganisms. The strong increase in Mn concentrations towards the bottom could be due to resuspension of clay particles and $MnO_2$ rich sediments driven by advection. Another possibility is Mn reduction in the sediments, followed by diffusion of $Mn^{2+}$ and reoxidation in bottom waters, consistent with elevated Mn/Fe ratios in bottom water. The general tendency of high correlations between S- and the trace metals Fe-Cu–Zn in the basin water was probably related to release of metal sulfide particles from the anoxic clay-organic sediments, whereas relative high Cu and Zn concentrations above sill depth point towards release from anthropogenic sources, which could be both industrial plants and aquaculture. Based on annual means at specific depths seston elemental stoichiometry (molar) were within the ranges: $C_{37-65}N_{8.4-31}P_1Si_{2-7.2}Ca_{2-4.5}O_{9.5-32}Fe_{0.2-2}Mn_{0.04-2.8}Zn_{0.13-0.8}S_{0.19-0.42}Cu_{0.02-0.19}Cl_{0.84-3.4}Na_{0.35-1.1}Mg_{0.29-1.6}K_{0.14-0.9}$, giving the overall average: $C_{55}N_{16}P_1Si_{3.6}Ca_{3.4}O_{16}Fe_{0.74}Mn_{0.51}Zn_{0.33}S_{0.21}Cu_{0.08}Cl_{1.7}Na_{0.68}Mg_{0.71}K_{0.37}$. It should be noted that the overall average gives N/P consistent with Redfield. As far as we are aware such deep water multielement relationships are novel for coastal areas and has value as reference far beyond its geographical area. It is to be expected that climate changes, such as increased precipitation and ice melting will lead to enhanced effluxes of PM and freshwater to the coastal regime, resulting in over representation of inorganic particles, deteriorating light climate, and stronger stratification due to reduced surface salinities.

**Data availability** The datasets generated during the current study are currently not publicly available but are available from the corresponding author on reasonable request.

**Declarations**

**Conflict of interest** The authors declare no conflict of interest.

# References

Aarseth I, Lønne Ø, Giskeødegaard O (1989) Submarine slides in glaciomarine sediments in some western Norwegian fjords. Mar Geol 88:1–21. https://doi.org/10.1016/0025-3227(89)90002-9

Aarseth I (1997) Western Norwegian fjord sediments: age, volume, stratigraphy, and role as temporary depository during glacial cycles. Mar Geol 143:39–53. https://doi.org/10.1016/S0025-3227(97)00089-3

Abdulgawad F, Bockelmann Evans BN, Sapsford D, Williams KP, Falconer RA (2008) Ammonium adsorption on clays and sand under freshwater and seawater conditions. In: Zhang C, Tang H (eds) Advances in water resources and hydraulic engineering. Proceedings of 16th IAHR-APD Congress and 3rd Symposium of IAHR-ISHS, pp 656–661, https://doi.org/10.1007/978-3-540-89465-0-115

Aksnes DL, Aure J, Kaartvedt S, Magnesen T, Richard J (1989) Significance of advection for the carrying capacities of fjord populations. Mar Ecol Prog Ser 50:263–274. https://doi.org/10.3354/meps050263

Andersen AT, Føyn L Jr (1969) Common methods for chemical analyses of seawater. In: Lange R (ed) Chemical oceanography. Scandinavian University Books, Oslo, pp 111–152

Arrigo KR (2005) Marine microorganisms and global nutrient cycles. Nature 437:349–355

Asplin L, Salvanes AGV, Kristoffersen JB (1999) Nonlocal wind-driven fjord–coast advection and its potential effect on plankton and fish recruitment. Fish Oceanogr 8:255–263. https://doi.org/10.1046/j.1365-2419.1999.00109.x

Asplin L, Albretsen J, Johnsen IA, Sandvik AD (2020) The hydrodynamic foundation for salmon lice dispersion modelling along the Norwegian coast. Ocean Dyn. https://doi.org/10.1007/s10236-020-01378-0

Aure J, Molvær J, Stigebrandt A (1996) Observations of inshore water exchange forced by a fluctuating offshore density field. Mar Pollut Bull 33:112–119. https://doi.org/10.1016/S0025-326X(97)00005-2

Aure J, Strand Ø, Erga SR, Strohmeier T (2007) Primary production enhancement by artificial upwelling in a western Norwegian fjord. Mar Ecol Prog Ser 352:39–52. https://doi.org/10.3354/meps07139

Bach LT, Boxhammer T, Larsen A, Hildebrandt N, Schulz KG, Riebesell U (2016) Influence of plankton community structure on the sinking velocity of marine aggregates. Global Biogeochem Cycles 30:1145–1165. https://doi.org/10.1002/2016GB005372

Barrón V, Torrent J (2013) Iron, manganese, and aluminium oxides and oxyhydroxides. EMU Notes Mineral 14:297–336

Barton CD, Karathanasis AD (2002) Clay minerals. In: Lal R (ed) Encyclopedia of soil science. Marcel Dekker Inc, New York, pp 187–192

Behera SK, Shukla AK (2014) Spatial distribution of surface soil acidity, electrical conductivity, soil organic carbon content and exchangeable potassium, calcium, and magnesium in some cropped acid soils of India. Land Degrad Dev 26:71–79. https://doi.org/10.1002/ldr.2306

Berg AS, Fauskanger L, Muggerud KK, Århus RH (2017) Hydropower: At the cost of the nature. Effects on hydrological and ecological conditions in the Sognefjord. Bachelor thesis, Sogn og Fjordane University College, p 136

Berg E, Albert OT (2003) Cod in fjords and coastal waters of North Norway: distribution and variation in length and maturity at age. ICES J Mar Sci 60:787–797. https://doi.org/10.1016/S1054-3139(03)00037-7

Bianchi TS, Arndt S, Austin WEN, Benn DI, Bertrand S, Cui X, Faust JC, Koziorowska-Makuch K, Moy CM, Savage C, Smeaton C, Smith RW, Syvitski J (2020) Fjords as aquatic critical zones (ACZs). Earth Sci Rev 203:103145. https://doi.org/10.1016/j.earscirev.2020.103145

Brzezinski MA (1985) The Si:C: N ratio of marine diatoms: interspecific variability and the effect of some environmental variables. J Phycol 21:347–357. https://doi.org/10.1111/j.0022-3646.1985.00347.x

Burgin AJ, Yang WH, Hamilton SK, Silver WL (2011) Beyond carbon and nitrogen: how the microbial energy economy couples elemental cycles in diverse ecosystems. Front Ecol Environ 9:44–52. https://doi.org/10.1890/090227

Cáceres JO, Sanz-Mangas D, Manzoor S, Pérez- Arribas LV, Anzano J (2019) Quantification of particulate matter, tracking the origin and relationship between elements for the environmental monitoring of the Antarctic region. Sci Total Environ 665:125–132. https://doi.org/10.1016/j.scitotenv.2019.02.116

Cho D-W, Chon C-M, Jeon B-H, Kim Y, Khan MA, Song H (2010) The role of clay minerals in the reduction of nitrate in groundwater by zero-valent iron. Chemosphere 81:611–616. https://doi.org/10.1016/j.chemosphere.2010.08.005

Chow C-ET, Kim DY, Sachdeva R, Caron DA, Fuhrman JA (2013) Top-down controls on bacterial community structure: microbial network analysis of bacteria, T4-like viruses and protists. ISME J. https://doi.org/10.1038/ismej.2013.199

Chrzanowski TH, Kyle M (1996) Ratios of carbon, nitrogen and phosphorus in *Pseudomonas fluorescens* as a model for bacterial elemental ratios and nutrient regeneration. Aquat Microb Ecol 10:115–122

Cleveland CC, Liptzin D (2007) C:N: P stoichiometry in soil: is there a "Redfield ratio" for the microbial biomass. Biogeochemistry 85:235–252. https://doi.org/10.1007/s10533-007-9132-0

Coelho FJRC, Santos AL, Coimbra J, Almeida A, Cunha Â, Cleary DFR, Calado R, Gomes NCM (2013) Interactive effects of global climate change and pollution on marine microbes: the way ahead. Ecol Evol 3:1808–1818. https://doi.org/10.1002/ece3.565

Crain CM, Halpern BS, Beck MW, Kappel CV (2009) Understanding and managing human threats to coastal marine environments. Ann NY Acad Sci 1162:39–62. https://doi.org/10.1111/j.1749-6632.2009.04496.x

Cram JA, Chow C-ET, Sachdeva R, Needham DM, Parada AE, Steele JA, Fuhrman JA (2015) Seasonal and interannual variability of the marine bacterioplankton community throughout the water column over ten years. ISME J 9:563–580. https://doi.org/10.1038/ismej.2014.153

Crawford DW, Wyatt SN, Wrohan IA, Cefarelli AO, Giesbrecht KE, Kelly B, Varela DE (2015) Low particulate carbon to nitrogen ratios in marine surface waters of the Arctic. Glob Biogeochem Cycles 29:2021–2033. https://doi.org/10.1002/2015GB005200

Diab S, Shilo M (1988) Effects of adhesion to particles on the survival and activity of *Nitrosomonas* sp. and *Nitrobacter* sp. Arch Microbiol 150:387–393. https://doi.org/10.1007/BF00408312

Ehn JK, Reynolds RA, Stramski D, Doxaran D, Lansard B, Babin M (2019) Patterns of suspended particulate matter across the continental margin in the Canadian Beaufort Sea during summer. Biogeosciences 16:1583–1605

Erga SR, Heimdal BR (1984) Ecological studies on the phytoplankton of Korsfjorden, western Norway. The dynamics of a spring bloom seen in relation to hydrographical conditions and light regime. J Plankton Res 6:67–90. https://doi.org/10.1093/plankt/6.1.67

Erga SR (1989) Ecological studies on the phytoplankton of Boknafjorden, western Norway. I. The effect of water exchange processes and environmental factors on temporal and vertical variability of biomass. Sarsia 74:161–176. https://doi.org/10.1080/00364827.1989.10413425

Erga SR, Aursland K, Frette Ø, Hamre B, Lotsberg JK, Stamnes JJ, Aure J, Rey F, Stamnes K (2005) UV transmission in Norwegian marine waters: controlling factors and possible effects on primary production and vertical distribution of phytoplankton. Mar Ecol Prog Ser 305:79–100. https://doi.org/10.3354/meps305079

Erga SR, Lie GC, Aarø LH, Aursland K, Olseng CD, Frette Ø, Hamre B (2010) Fine scale vertical displacement of *Phaeodactylum tricornutum* (Bacillariophyceae) in stratified waters: influence of halocline and day length on buoyancy control. J Exp Mar Biol Ecol 384:7–17. https://doi.org/10.1016/j.jembe.2009.11.017

Erga SR, Ssebiyonga N, Frette Ø, Hamre B, Aure J, Strand Ø, Strohmeier T (2012) Dynamics of phytoplankton distribution and photosynthetic capacity in a western Norwegian fjord during coastal upwelling: effects on optical properties. Estuar Coast Shelf Sci 97:91–103. https://doi.org/10.1016/j.ecss.2011.11.034

Erga SR, Ssebiyonga N, Hamre B, Frette Ø, Hovland E, Hancke K, Drinkwater K, Rey F (2014) Environmental control of phytoplankton distribution and photosynthetic performance at the Jan Mayen Front in the Norwegian Sea. J Mar Syst 130:193–205

Erga SR, Lie GC, Aarø LH, Frette Ø, Hamre B (2015) Migratory behaviour of *Skeletonema grethae* (Bacillariophyceae) in stratified waters. Diat Res 30:13–25. https://doi.org/10.1080/0269249X.2014.943808

Erga SR, Haugen SB, Bratbak G, Egge JK, Heldal M, Mork KA, Norland S (2017) Seasonal variations in C:N:Si:Ca:P:Mg:S:K: Fe relationships of SPM from Norwegian coastal water: impact of extreme offshore forcing during winter-spring 2010. Mar Chem 196:1–12. https://doi.org/10.1016/j.marchem.2017.07.001

Eturki S, Ayari F, Jedidi N, Dhia HB (2012) Use of clay mineral to reduce ammonium from wastewater. Effects of various parameters. Surf Eng Appl Electrochem 48:276–283. https://doi.org/10.3103/S1068375512030064

Fagerbakke KM, Heldal M, Norland S, Heimdal BR, Batvik H (1994) *Emiliania huxleyi*. Chemical composition and size of coccoliths from enclosure experiments and a Norwegian fjord. Sarsia 79:349–355. https://doi.org/10.1080/00364827.1994.10413566

Fagerbakke KM, Heldal M, Norland S (1996) Content of carbon, nitrogen, oxygen, sulfur and phosphorus in native aquatic and cultured bacteria. Aquat Microb Ecol 10:15–27

Faust JC, Knies J, Milzer G, Giraudeau J (2014) Terrigenous input to a fjord in central Norway records the environmental response to the North Atlantic Oscillation over the past 50 years. The Holocene 24:1411–1418. https://doi.org/10.1177/0959683614544052

Faust JC, Scheiber T, Fabian K, Vogt C, Knies J (2017) Geochemical characterization of northern Norwegian fjord surface sediments: a baseline for further paleo-environmental investigations. Cont Shelf Res 148:104–115. https://doi.org/10.1016/j.csr.2017.08.015

Fosså JH, Brattegard T (1990) Bathymetric distribution of Mysidacea in fjords of western Norway. Mar Ecol Prog Ser 67:7–18. https://doi.org/10.3354/meps067007

Gašparović B, Penezeić A, Frka S, Kazazić S, Lampitt RS, Holguin FO, Sudasinghe N, Schaub T (2018) Particulate sulfur-containing lipids: production and cycling from the epipelagic to the abyssopelagic zone. Deep-Sea Res I 134:12–22. https://doi.org/10.1016/j.dsr.2018.03.007

Gebser B, Thume K, Steinke M, Pohnert G (2020) Phytoplankton-derived zwitterionic gonyol and dimethylsulfonioacetate interference with microbial dimethylsulfoniopropionate sulfur cycling. MicrobiologyOpen 2020:e1014. https://doi.org/10.1002/mbo3.1014

Gilbert JA, Steele JA, Caporaso JG, Steinbrück L, Reeder J, Temperton B, Huse S, McHardy AC, Knight R, Joint I (2012) Defining seasonal marine microbial community dynamics. ISME J 6:298–308. https://doi.org/10.1038/ismej.2011.107

Grefsrud ES, Glover K, Grøsvik BE, Husa V, Karlsen Ø, Kristiansen T, Kvamme BO, Mortensen S, Samuelsen OB, Stien LH, Svåsand T (2018) Risk assessment report norwegian aquaculture 2018 (In Norwegian). Fisken og Havet (Inst Mar Res Bergen), særnr 1–2018, p 182

Grøttå HM, Rødland J, Trefall K (2016) Alterations of the runoff pattern in rivers in Indre Sogn as a result of hydroelectric power production. Bachelor thesis, Sogn og Fjordane University College, p 92

Gutiérrez MH, Galand PE, Moffat C, Pantoja S (2015) Melting glacier impacts community structure of Bacteria, Archaea and Fungi in a Chilean Patagonia fjord. Environ Microbiol 17:3882–3897. https://doi.org/10.1111/1462-2920.12872

Gutiérrez MH, Narváez D, Daneri G, Montero P, Pérez-Santos I, Pantoja S (2018) Linking seasonal reduction of microbial diversity to increase in winter temperature of waters of a Chilean Patagonia fjord. Front Mar Sci 5:277. https://doi.org/10.3389/fmars.2018.00277

Heldal M, Scanlan DJ, Norland S, Thingstad F, Mann NH (2003) Elemental composition of single cells of various strains of marine *Prochlorococcus* and *Synechococcus* using X-ray microanalysis. Limnol Oceanogr 48:1732–1743

Heldal M, Norland S, Erichsen ES, Sandaa R-A, Larsen A, Thingstad F, Bratbak G (2012) $Mg^{2+}$ as indicator of nutritional status in marine bacteria. ISME J 6:524–530

Helliwell KE, Harrison EL, Christie-Oleza JA, Rees AP, Kleiner FH, Gaikwad T, Downe J, Aguilo-Ferretjans MM, Al-Moosawi L, Brownlee C, Wheeler GL (2021) A novel $Ca^{2+}$ signaling pathway coordinates environmental phosphorus sensing and nitrogen metabolism in marine diatoms. Curr Biol 31:978–989

Holmes RM, Aminot A, Kerouel R, Hooker BA, Peterson BJ (1999) A simple and precise method for measuring ammonium in marine and freshwater ecosystems. Can J Fish Aquat Sci 56:1801–1808. https://doi.org/10.1139/f99-128

Inall ME, Gillibrand PA (2010) The physics of mid-latitude fjords: a review. In: Howe JA, Austin WEN, Forwick M, Paetzel M (eds) Fjord systems and archives, vol 344. Geological Society, London, pp 17–33

Johnson DR (1977) Determining vertical velocities during upwelling off the Oregon coast. Deep-Sea Res 24:171–180. https://doi.org/10.1016/0146-6291(77)90551-3

Klitgaard-Kristensen D, Buhl-Mortensen L (1999) Benthic foraminifera along an offshore-fjord gradient: a comparison with amphipods and molluscs. J Nat Hist 33:317–350. https://doi.org/10.1080/002229399300281

Lam PJ, Ohnemus DC, Marcus MA (2012) The speciation of marine particulate iron adjacent to active and passive continental margins. Geochim Cosmochim Acta 80:108–124. https://doi.org/10.1016/j.gca.2011.11.044

Larsen A, Flaten GAF, Sandaa R-A, Castberg T, Thyrhaug R, Erga SR, Jacquet S, Bratbak G (2004) Spring phytoplankton bloom dynamics in Norwegian coastal waters: microbial community succession and diversity. Limnol Oceanogr 49:180–190. https://doi.org/10.4319/lo.2004.49.1.0180

Liebes SM (1992) An introduction to marine biogeochemistry. Wiley, New York, p 734

Liermann LJ, Hausrath EM, Anbar AD, Brantley SL (2007) Assimilatory and dissimilatory processes of microorganisms in the environment. J Anal Spectrom 22:867–877. https://doi.org/10.1039/B705383E

Maechler M, Rousseeuw P, Struyf A, Hubert M, Hornik K (2019) Cluster: cluster Analysis Basics And Extensions v.1.14

Manzetti S, Stenersen JHV (2010) A critical view of the environmental condition of the Sognefjord. Mar Pollut Bull 60:2167–2174. https://doi.org/10.1016/j.marpolbul.2010.09.019

Marie D, Brussaard CP, Thyrhaug R, Bratbak G, Vaulot D (1999) Enumeration of marine viruses in culture and natural samples by flow cytometry. Appl Environ Microbiol 65:45–52. https://doi.org/10.1128/AEM.65.1.45-52.1999

Marie D, Partensky F, Vaulot D, Brussaard C (2001) Enumeration of phytoplankton, bacteria, and viruses in marine samples. Curr Protoc Cytom. https://doi.org/10.1002/0471142956.cy1111s10

Martin DD, Ciulla RA, Roberts MF (1999) Osmoadaptation in archaea. Appl Environ Microbiol 65:1815–1825

Martiny AC, Vrugt JA, Lomas MW (2014) Concentrations and ratios of particulate organic carbon, nitrogen, and phosphorus in the global ocean. Sci Data 1:140048. https://doi.org/10.1038/sdata.2014.48

Merchant SS, Helmann JD (2012) Elemental economy: microbial strategies for optimizing growth in the face of nutrient limitation. Adv Microb Physiol 60:91–210. https://doi.org/10.1016/B978-0-12-398264-3.00002-4

Myksvoll MS, Sandvik AD, Asplin L, Sundby S (2014) Effects of river regulations on fjord dynamics and retention of coastal cod eggs. ICES J Mar Sci 71:943–956. https://doi.org/10.1093/icesjms/fst113

Ndzana GM, Huang L, Zhang Z, Zhu J, Liu F, Bhattacharyya R (2019) The transformation of clay minerals in the particle size fractions of two soils from different latitude in China. CATENA 175:317–328. https://doi.org/10.1016/j.catena.2018.12.026

Nolting RF (1986) Copper, zinc, cadmium, nickel, iron and manganese in the Southern Bight of the North Sea. Mar Poll Bul 17:113–117. https://doi.org/10.1016/0025-326X(86)90415-7

Oksanen J, Guillaume Blanchet F, Friendly M, Kindt R, Legendre P, McGlinn D, Minchin PR, O'Hara RB, Simpson GL, Solymos P, Stevens MHH, Szoecs E, Wagner H (2020) vegan: community ecology package. R package version 2.5-7. https://CRAN.R-project.org/package=vegan

Paasche E (1980) Silicon content of five marine plankton diatom species measured with a rapid filter method. Limnol Oceanogr 25:474–480. https://doi.org/10.4319/lo.1980.25.3.0474

Paasche E, Erga SR (1988) Phosphorus and nitrogen limitation of phytoplankton in the inner Oslofjord (Norway). Sarsia 73:229–243. https://doi.org/10.1080/00364827.1988.10413409

Paasche E (2002) A review of the coccolithophorid *Emiliania huxleyi* (Prymnesiophyceae), with particular reference to growth, coccolith formation, and calcification-photosynthesis interactions. Phycologia 40:503–529. https://doi.org/10.2216/i0031-8884-40-6-503.1

Paetzel M, Dale T (2010) Climate proxies for recent fjord sediments in the inner Sognefjord region, Western Norway. Geol. Soc. Lond. Spec. Publ. 344:271–288. https://doi.org/10.1144/SP344.19

Paradis E, Schliep K (2019) Ape 5.0: an environment for modern phylogenetics and evolutionary analyses in R. Bioinformatics 35:526–528. https://doi.org/10.1093/bioinformatics/bty633

Parsons TR, Maita Y, Lalli CM (1992) A manual of chemical and biological methods for sea water analysis. Pergamon Press, New York, p 173

Paulino AI, Heldal M, Norland S, Egge JK (2013) Elemental stoichiometry of marine particulate matter measured by wavelength dispersive X-ray fluorescence (WDXRF). J Mar Biol Assoc 93:2003–2014. https://doi.org/10.1017/S0025315413000635

Peperzac L, Colun F, Koeman R, Gieskes WWC, Joordens JCA (2003) Phytoplankton sinking rates in the Rhine region of freshwater influence. J Plankton Res 25:365–383

Pomeroy LR, Williams PJB, Azam F, Hobbie JE (2007) The microbial loop. Oceanography 20:28–33. https://doi.org/10.5670/oceanog.2007.45

Poulin P, Pelletier E (2007) Determination of ammonium using a microplate-based fluorometric technique. Talanta 71:1500–1506. https://doi.org/10.1016/j.talanta.2006.07.024

Pree B, Larsen A, Egge JK, Simonelli P, Madhusoodhanan R, Tsagaraki TM, Våge S, Erga SR, Bratbak G, Thingstad TF (2017) Dampened copepod-mediated trophic cascades in a microzooplankton-dominated microbial food web: a mesocosm study. Limnol Oceanogr 62:1031–1044. https://doi.org/10.1002/lno.10483

Price NB, Skei JM (1975) Areal and seasonal variations in the chemistry of suspended particulate matter in a deep water fjord. Estuar Coast Mar Sci 3:349–369. https://doi.org/10.1016/0302-3524(75)90034-1

Raven JA (2017) Chloride: essential micronutrient and multifunctional beneficial ion. J Exp Bot 68:359–367. https://doi.org/10.1093/jxb/erw421

Redfield AC, Ketchum BH, Richards FA (1963) The influence of organisms on the composition of seawater. In: Hill MN (ed) The Sea, vol 2. Interscience, New York, pp 26–77

Rees AP, Woodward EMS, Joint I (2006) Concentrations and uptake of nitrate and ammonium in the Atlantic Ocean between 60 degrees N and 50 degrees S. Deep Sea Res. Part II. Top Stud Oceanogr 53:1649–1665

Reynolds RA, Stramski D, Wright VM, Woźniak SB (2010) Measurements and characterization of particle size distribution in coastal waters. J Geophys Res 115:C08024. https://doi.org/10.1029/2009JC005930

Schneider B, Schlitzer R, Fisher G, Nöthig EM (2003) Depth-dependent elemental composition of particulate organic matter (POM) in the ocean. Glob Biogeochem Cycles 17(2):1032. https://doi.org/10.1029/2002GB001871

Sdiri AT, Higashi T, Jamoussi F (2014) Adsorption of copper and zinc onto natural clay in single and binary systems. Int J Environ Sci Technol 11:1081–1092. https://doi.org/10.1007/s13762-013-0305-1

Seitz AC, Michalsen K, Nielsen JL, Evans MD (2014) Evidence of fjord spawning by southern Norwegian Atlantic halibut (*Hippoglossus hippoglossus*). ICES J Mar Sci 71:1142–1147. https://doi.org/10.1093/icesjms/fst227

Sharoni S, Halevy I (2020) Nutrient ratios in marine particulate organic matter are predicted by the population structure of well-adapted phytoplankton. Sci Adv 6:eaaw9371. https://doi.org/10.1126/sciadv.aaw9371

Skagseth Ø, Slotte A, Stenevik EK, Nash RDM (2015) Characteristics of the Norwegian Coastal Current during years with high recruitment of Norwegian Spring Spawning Herring (*Clupea harengus* L.). PLoS ONE 10(12):e0144117. https://doi.org/10.1371/journal.pone.0144117

Skarbøvik E, Allan I, Sample JE, Greipsland I, Selvik JR, Schanke LB, Beldring S, Stålnacke P, Kaste Ø (2017) Riverine inputs and direct discharges to Norwegian coastal waters—2016. NIVA Report 7217-2017, ISBN: 978-82-677-6952-9, p 85

Skei JM, Loring DH, Rantala RTT (1996) Trace metals in suspended particulate matter and in sediment trap material from a permanently anoxic fjord—Framvaren, South Norway. Aquat Geochem 2:131–147. https://doi.org/10.1007/BF00121628

Stabholz M, Durrieu de Madron X, Canals M, Khripounoff A, Taupier-Letage I, Testor P, Heussner S, Kerhervé P, Delsaut N, Houpert L, Lastras G, Dennielou B (2013) Impact of open-ocean convection on particle fluxes and sediment dynamics in the deep margin of Gulf of Lions. Biogeosciences 10:1097–1116. https://doi.org/10.5194/bg-10-1097-2013

Sterner R, Elser JJ (2002) Ecological stoichiometry: the biology of elements from molecules to biosphere. Princeton University Press, Princeton, p 464

Stigebrandt A, Aure J (1989) Vertical mixing in basin waters of fjords. J Phys Oceanogr 19:917–926. https://doi.org/10.1175/1520-0485(1989)019%3c0917:VMIBWO%3e2.0.CO;2

Storesund JE, Erga SR, Ray JL, Thingstad TF, Sandaa RA (2015) Top-down and bottom-up control on bacterial diversity in a western Norwegian deep-silled fjord. FEMS Microbiol Ecol 91:1–10. https://doi.org/10.1093/femsec/fiv076

Storesund JE, Sandaa RA, Thingstad TF, Asplin L, Albretsen J, Erga SR (2017) Linking bacterial community structure to advection and environmental impact along a coast-fjord gradient of the Sognefjord, western Norway. Prog Oceanogr 159:13–30. https://doi.org/10.1016/j.pocean.2017.09.002

Støylen E, Fer I (2014) Tidally induced internal motion in an Arctic fjord. Nonlinear Processes Geophys 21:87–100. https://doi.org/10.5194/npg-21-87-2014

Sutherland BR, Barrett KJ, Gingras MK (2014) Clay settling in fresh and salt water. Environ Fluid Mech. https://doi.org/10.1007/s10652-014-9365-0

Suttle CA (2007) Marine viruses–major players in the global ecosystem. Nat Rev Microbiol 5:801–812. https://doi.org/10.1038/nrmicro1750

Svendsen H (1981) A study of circulation and exchange processes in the Ryfylkefjords. Rep., 55. Geophys Inst University of Bergen, Bergen, p 140

Sætre R, Gjertsen K, Bröker K (2007) The Norwegian coastal current: oceanography and climate. Tapir Academic Press, Trondheim, p 159

Taiz L, Zeiger E (2006) Plant physiology, 4th edn. Sinauer Associates Inc Publishers, Sunderland, p 764

Tan X, Zhang G, Yin H, Reed AH, Furukawa Y (2012) Characterization of particle size and settling velocity of cohesive sediments affected by a neutral exopolymer. Int J Sediment Res 27:473–485. https://doi.org/10.1016/S1001-6279(13)60006-2

Thamdrup B, Dalsgaard T (2000) The fate of ammonium in anoxic manganese oxide-rich marine sediment. Geochim Cosmochim Acta 64:4157–4164. https://doi.org/10.1016/S0016-7037(00)00496-8

They NH, Amado AM, Cotner JB (2017) Redfield ratios in Inland waters: higher biological control of C:N: P ratios in tropical semi-arid high water residence time lakes. Front Microbiol 8:1505. https://doi.org/10.3389/fmicb.2017.01505

Vandieken V, Pester M, Finke N, Hyun JH, Friedrich MW, Loy A, Thamdrup B (2012) Three manganese oxide-rich marine sediment harbor similar communities of acetate-oxidizing manganese-reducing bacteria. ISME J 6:2078–2090. https://doi.org/10.1038/ismej.2012.41

Van Raaphorst W, Malschaert JFP (1996) Ammonium adsorption in superficial North Sea sediments. Cont Shelf Res 16:1415–1435

Vélez-Belchí P, Tintoré J (2001) Vertical velocities at an ocean front. Sci Mar 65:291–300. https://doi.org/10.3989/scimar.2001.65s1291

Wassmann P (1984) Sedimentation and benthic mineralization of organic detritus in a Norwegian fjord. Mar Biol 83:83–94. https://doi.org/10.1007/BF00393088

Weinbauer MG, Hornák K, Jezbera J, Nedoma J, Dolan JR, Šimek K (2007) Synergistic and antagonistic effects of viral lysis and protistan grazing on bacterial biomass, production, and diversity. Environ Microbiol 9:777–788. https://doi.org/10.1111/j.1462-2920.2006.01200.x

Winkelmann D, Knies J (2005) Recent distribution and accumulation of organic carbon on the continental margin west off Spitsbergen. Geochem Geophys Geosyst 6:Q09012. https://doi.org/10.1029/2005GC000916